USGS
science for a changing world

ARRA-Funded V_{S30} Measurements Using Multi-Technique Approach at Strong-Motion Stations in California and Central-Eastern United States

Open-File Report 2013–1102

U.S. Department of the Interior
U.S. Geological Survey

This page intentionally left blank

USGS
science for a changing world

ARRA-Funded V_{S30} Measurements Using Multi-Technique Approach at Strong-Motion Stations in California and Central-Eastern United States

By Alan Yong, Antony Martin, Kenneth Stokoe, and John Diehl

Open-File Report 2013–1102

U.S. Department of the Interior
U.S. Geological Survey

U.S. Department of the Interior
SALLY JEWELL, Secretary

U.S. Geological Survey
Suzette M. Kimball, Acting Director

U.S. Geological Survey, Reston, Virginia: 2013

Suggested citation:
Yong, A., Martin, A., Stokoe, K., and Diehl, J., 2013, ARRA-funded V_{S30} measurements using multi-technique approach at strong-motion stations in California and central-eastern United States: U.S. Geological Survey Open-File Report 2013–1102, 59 p. and data files, *http://pubs.usgs.gov/of/2013/1102/*.

Contents

Figures

Tables

ARRA-Funded V_{S30} Measurements Using Multi-Techniques at Strong-Motion Stations in California and Central-Eastern United States

By Alan Yong[1], Antony Martin[2], Kenneth Stokoe[3], and John Diehl[2]

Abstract

Funded by the 2009 American Recovery and Reinvestment Act (ARRA), we conducted geophysical site characterizations at 191 strong-motion stations: 187 in California and 4 in the Central-Eastern United States (CEUS). The geophysical methods used at each site included passive and active surface-wave and body-wave techniques. Multiple techniques were used at most sites, with the goal of robustly determining V_S (shear-wave velocity) profiles and V_{S30} (the time-averaged shear-wave velocity in the upper 30 meters depth). These techniques included: horizontal-to-vertical spectral ratio (HVSR), two-dimensional (2-D) array microtremor (AM), refraction microtremor (ReMi^{TM}), spectral analysis of surface wave (SASW), multi-channel analysis of surface waves (Rayleigh wave: MAS_RW; and Love wave: MAS_LW), and compressional- and shear-wave refraction. Of the selected sites, 47 percent have crystalline, volcanic, or sedimentary rock at the surface or at relatively shallow depth, and 53 percent are of Quaternary sediments located in either rural or urban environments. Calculated values of V_{S30} span almost the full range of the National Earthquake Hazards Reduction Program (NEHRP) Site Classes, from D (stiff soils) to B (rock). The NEHRP Site Classes based on V_{S30} range from being consistent with the Class expected from analysis of surficial geology, to being one or two Site Classes below expected. In a few cases where differences between the observed and expected Site Class occurred, it was the consequence of inaccurate or coarse geologic mapping, as well as considerable degradation of the near-surface rock. Additionally, several sites mapped as rock have Site Class D (stiff soil) velocities, which is due to the extensive weathering of the surficial rock.

[1] U.S. Geological Survey
[2] GEOVision, Inc.
[3] University of Texas, Austin

1.0 Introduction

With funding from the 2009 American Recovery and Reinvestment Act (ARRA, *http://www.recovery.gov/;* accessed June 27, 2012), the U.S. Geological Survey solicited proposals to characterize geotechnical site conditions at 197 strong-motion (SM) stations in California and the central-eastern United States (fig. 1 and table 1).

A consortium of academic researchers and commercial collaborators, consisting of principals from the University of Texas, Austin, and GEOVision©, Inc., competitively responded to the U.S. Geological Survey's request for proposal and, in March 2010, the consortium was awarded a contract for 191 stations (table 1).

The project had two objectives: (1) to acquire a range of site-specific geophysical data for the ground motion modeling community, and (2) to establish a pilot project for the Advanced National Seismic System to guide similar efforts in the future. The most important task in this site characterization project was the determination of the geotechnical parameter V_{S30}, the time-averaged shear-wave velocity (V_S) in the upper 30 m. Despite its inherent limitations (Boore, 2004; Mucciarelli and Gallipoli, 2006; Bragato, 2008; Castellaro and others, 2008; Lee and Trifunac, 2010), V_{S30} is presently used as the single explanatory variable for describing the influence of local conditions on ground motions (Boore and others, 1993, 1994, 1997; Abrahamson and others, 2008). It is also widely used as the basis for establishing building codes (Borcherdt, 1994; Dobry and others, 2000; Building Seismic Safety Council, 2003; Eurocode 8, 2004), and for developing modern microzonation maps (Scott and others, 2006; Castellaro and Mulargia, 2009; Thompson and others, 2010; Yong and others, 2011). In addition to the estimates of V_{S30}, the observations and experience gained from this project are expected to yield guidelines for using indirect or non-invasive geophysical techniques to characterize site conditions.

The 187 stations investigated in California represent 6 different seismographic networks: 131 are operated by the Southern California Seismic Network (SCSN), 2 by the U.C. Berkeley Digital Seismic Network, 3 by the utility Pacific Gas and Electric, 25 by the Northern California Seismic Network, 25 by the California Geological Survey, and 1 by the University of California San Diego's ANZA seismic network (fig. 1 and table 1). These sites were selected on the basis of their expected exceedance of ground motions (peak ground acceleration for 10 percent in 50 years) as estimated by Petersen and others (2008). Four Central-Eastern United States (CEUS) sites were included to demonstrate that these techniques could be used outside of California.

Fieldwork and data analysis took more than 2 years to complete (March 1, 2010–May 31, 2012). In this report, we describe the range of techniques that were used to investigate the sites and the strategies used to overcome problems encountered in the data acquisition and analysis components of the project (see "Methods" in Section 2.0). For results, we summarize our preliminary observations (see "Results" in Section 3.0) and present individual site reports (see appendix A) where details about the geophysical results and models that were developed for each SM station can be found.

2.0 Methods

Various non-invasive geophysical survey methods—consisting of passive and active surface- and body-wave techniques—were applied at each station (tables 2 and 3). The following sections describe the prerequisites to field survey, the individual techniques applied, the basis for applying one or more established techniques (table 2), and the procedures for field acquisition and data analysis. Details on site-specific applications, as well as any deviation(s) from standardized procedures, are described in the "Observations/Discussion" section of each site report (appendix A).

2.1 Prerequisites to Field Surveys

In addition to strict requirements specified by the ARRA legislation, three conditions were imposed on the contractors to address concerns about scientific rigor and issues relating to cost and environmental impact. These mandates included: prerequisites on site selection for the measurement arrays prior to each site visit, metrics on distances between the array(s) and the station, and restrictions on types of geophysical survey methods.

The first requirement was designed to minimize the amount of time spent at each station. Details about a station, determined using map-based satellite imagery and geology, must first be approved by the U.S. Geological Survey prior to deployment of geophysical arrays at the site. For every station, maps (as shown in fig. 2) include a red dot marking the known (on record) location of the SM instrumentation, a green circle delineating the 150-m radial distance from the SM site, a blue circle indicating the 300-m maximum radial extent, and red line(s) describing the proposed location(s) of the recording array(s) to be deployed during the survey.

To acquire the best possible interpretation of the velocity profile directly beneath each station, a second requirement restricted the locations of measurement arrays to within 150-m radial distance from the known locations (on record) of the SM instrument. However, when elements, such as man-made impediments (parked vehicles, temporary or permanent structures, permission-related access issues, etc.) or geophysical constraints (irregular surface topography, steep slope gradient, etc.), within the 150-m radial area, prohibited the effective deployment of the array, we followed the recommendation of Borcherdt (2002) to allow an extension of the radius to no more than 300 m from the SM instrument. A necessary condition for such an exception was that the surficial geologic materials surrounding the station should be verified as matching, or closely matching, the materials at the location of the proposed array.

The third requirement restricts field survey methods to non-invasive geophysical techniques, either in combination (preferred) or as standalone. Non-invasive methods have become popular because, in contrast to traditional down-hole methods, they do not require expensive and time consuming drilling of boreholes. Given that almost all SM stations are hosted by public and private entities, non-invasive techniques were deemed best suited for characterizing site conditions in such sensitive settings. The major drawback for non-invasive methods, however, is that these techniques determine seismic properties indirectly by inversion of surface-wave phase velocity to estimate body-wave velocity, and hence tend to introduce more uncertainty into the estimated values than invasive approaches (Boore, 2006; Moss, 2008). Nevertheless, by comparing results from

multiple techniques the inherent uncertainties can be significantly reduced (Boore, 2006; Cornou and others, 2006; Foti and others, 2007; Cakir and Walsh, 2009; Odum and others, 2010; Comina and others, 2011; Cakir and Walsh, 2012).

2.2 Geophysical Techniques

Eight geophysical techniques were used in this project (table 2). These included active surface-wave techniques (spectral analysis of surface waves [SASW] and multi-channel analysis of surface waves [MASW] using both Rayleigh [MAS_RW] and Love [MAS_LW] waves), passive surface-wave techniques (horizontal-to-vertical spectral ratio [HVSR], array microtremor [AM], and refraction microtremor [ReMi™]), and seismic refraction of both P- and S-waves. Each technique was used either as a standalone method or, whenever applicable, as part of a multi-method approach (tables 2 and 3) that combined complementary techniques. For each SM station, V_S models and V_{S30} values are then determined on the basis of one, a subset, or all these techniques.

In this report, we briefly describe each geophysical technique and highlight details that are pertinent to this project. References that fully explain the techniques are provided and, whenever possible, include the main developers of each approach.

(Note: In the individual site reports, MASW and MALW refer to MAS_RW and MAS_LW, respectively; see Glossary for de-abbreviations).

2.2.1 Active Surface-Wave Methods

Active surface-wave methods, such as SASW and MASW, are proven non-destructive geophysical techniques for determining the variation of V_S with depth (Stokoe and others, 1994; Brown and others, 2000; Park and others, 1999; Foti and others, 2007). Measurements are made on the ground surface at strain levels in the elastic range (< 0.001 percent) (Holtz and others, 2010). Surface-wave surveys consist of recording Rayleigh-wave phase velocity (V_R) and/or Love-wave phase velocity (V_L) data in the field, generating a dispersion curve, and then using iterative forward- and/or inverse-modeling techniques to determine the corresponding V_S model and V_{S30} value. These techniques, particularly those utilizing Rayleigh waves, have undergone significant research and development over many decades (Stokoe and others, 1988; Park and others, 1999; Zywicki, 1999; Park and others, 2005; Stokoe and others, 2006; Strobbia and Foti, 2006; Cox and Wood, 2011) since the seminal works of Aki (1957, 1965). Although Love waves have been utilized in seismological studies for many years (for example, Lay and Wallace, 1995), the application of Love wave recordings to geotechnical investigations is only recently gaining traction. Consequently, the literature is sparse on topics such as spectral analysis (SAS_LW) and multi-channel analysis (MAS_LW) of Love waves. To our knowledge, one of the earliest applications of Love waves for characterizing near surface V_S structure is by Mari (1984). Later, a computational basis for the spectral analysis of Love waves was presented in Guzina and Madyarov (2003). More recent publications describing the application of MAS_LW include Safani and others (2005), Eslick and others (2007), Pei (2007), Schuler (2008), Lane (2009), and Xia and others (2012).

2.2.1.1 SASW Technique

The seismic source for the SASW method is a vertical dynamic load that generates horizontally propagating Rayleigh waves. Ground motions are monitored by two vertical receivers and recorded by a data acquisition system capable of producing records in both time and frequency domains. Theoretical as well as practical considerations (attenuation, near-field effects, and spatial aliasing) necessitate the use of different receiver intervals to generate the dispersion curve over the wavelength range required to determine the V_S profile. To develop a V_S model to a 30-m depth, energy sources typically include: small hammers (rock hammer or 3-lb hammer) for short receiver intervals; 10- to 20-lb sledge hammers for intermediate separations, and accelerated weight drops (AWD) or an electromechanical shaker for larger spacings. More energetic sources, such as bulldozers or seismic vibrators (Vibroseis™), can be used to characterize velocity structures to depths of 100 m or more. Generally, high frequency (short wavelength) surface waves are recorded across receiver pairs spaced at short intervals, whereas low frequency (long wavelength) surface waves require greater spacing between receivers. Dispersion data averaged across greater distances are often smoother because effects of localized heterogeneities are averaged.

Two source-receiver configurations typically used for acquiring SASW data are the common-midpoint (fixed center point for expanding receiver array) and the common-source (fixed source location, moving receivers) geometries. The common-receiver midpoint geometry has a distinct advantage at sites with lateral velocity variation because all receiver pairs sample an overlapping region of the array. In order to minimize near-field effects associated with the cylindrical (as opposed to planar; see Section 2.2.1.2) wave-front, while also ensuring a good signal-to-noise ratio, the distance between the source and near receiver typically is set to be equal to the receiver spacing (Sánchez-Salinero, 1987; Nazarian and Desai, 1993). The source location is generally reversed (Stokoe and others, 1994) to assess the effects of small phase shifts between sensors and the lateral velocity variation.

The time-domain records from the two receivers are converted to the frequency-domain by calculating the Fast Fourier Transform, the cross power spectrum, and the coherence. The frequency-dependent phase of the cross-power spectrum, $\phi_w(f)$, represents the phase differences (between $-\pi$ and π) from the two receivers as the wave train passes through. Because the phase differences are in wrapped form, they must be unwrapped to form a continuous function of frequency versus phase angle. During the unwrapping process, near-field data (typically wavelengths longer than twice the distance from the source to near receiver) and low-coherence data are discarded. The experimental dispersion curve, as a function of the unwrapped phase angle and the distance between receivers, is calculated as:

$$V_R = f \frac{d_2}{\frac{\Delta\phi}{360^\circ}}$$

where, V_R is Rayleigh wave phase velocity, f is frequency, d_2 is the distance between receivers, and $\Delta\phi$ is the phase difference in degrees. This process is repeated for each receiver spacing and individual dispersion curves are combined to form a composite dispersion curve. This composite dispersion curve is typically resampled and smoothed to

form a representative dispersion curve, which is utilized for forward and/or inverse modeling. A more detailed description of the SASW technique is provided in Joh (1996).

2.2.1.2 MASW (MAS_RW and MAS_LW) Techniques

In MASW techniques, surface waves are recorded by a linear array of 24 or more geophones typically spaced 1- to 3-m apart. Vertical and horizontal energy sources range from small hammers to large weight drops and vibratory sources. When applying the MASW technique to develop a one-dimensional (1-D) V_S model (see Subsection 2.2.3), surface-wave data are preferably acquired using multiple-source offsets at both ends of the array. A wave-field transform is applied to the time-history data to convert the seismic record from a time-distance space to a phase velocity-frequency space in which the surface-wave dispersion curve can be easily identified. Common wave-field transforms include the frequency-wavenumber (*f-k*) transform, the slant-stack transform (McMechan and Yedlin, 1981), and the phase-shift transform (Park and others, 1998). Another method for obtaining the surface-wave dispersion curve includes multi-offset phase analysis (Strobbia and Foti, 2006).

The *f-k* transform, which is a two-dimensional (2-D) Fourier transform over the time and space domain, can be very easily implemented in computer programs, such as MATLAB™, and is therefore commonly utilized. The phase-shift transform is implemented in many commercially developed geophysical software packages designed for surface-wave analysis. The slant-stack (τ-p) transform is exclusively used in geophysical signal processing, but has the disadvantage of lower resolution compared to the phase-shift transform (Park and others, 1998).

MASW and SASW data are subject to near-field effects resulting from the non-planar wave-front (Lai and Rix, 1998; Scocco and others, 2002). Near-field effects in MAS_RW data have been the subject of significant research in recent years (O'Neill, 2003; Zywicki and Rix, 2005; Xu and Miller, 2006; Bodet and others, 2009; Yoon and Rix, 2009; Li and Rosenblad, 2011). Although the results of these studies vary, they nonetheless demonstrate that near-field effects can result in significantly underestimated Rayleigh-wave phase velocities at wavelengths greater than one-half the receiver-spread length for linear arrays (Bodet and others, 2009), at wavelengths greater than the mean-source to receiver distance (Yoon and Rix, 2009), or at wavelengths greater than twice the mean source to receiver distance (Li and Rosenblad, 2011). Of course, field logistics dictate that having a receiver geometry adequate for mitigating near-field effects has to be balanced against the disadvantages of longer receiver arrays (such as the loss of high-frequency dispersion data, the significant contribution of lateral-velocity variation, and increased signal attenuation). The cylindrical beam-forming method of Zywicki (1999) and Zywicki and Rix (2005) offers a means to address the inconsistency between the cylindrical- and plane-wave assumptions used in the wavefield transformation process; however, the routine is currently not readily available. Multi-offset phase analysis, as described by Strobbia and Foti (2006), can help distinguish between near-field effects, lateral velocity variation, and higher mode contamination in MAS_RW data.

As discussed earlier, applications of Love-wave methods at the geotechnical scale have a much shorter history than Rayleigh-wave based methods. For this reason, much of the basic applied research (near-field effects; optimal survey design; source-frequency limitations, such as the low-frequency limits of a hammer and plank source; strengths and

limitations) has yet to be discussed in published literature. Many large, low-frequency sources utilized for deep SASW soundings (such as bulldozers and large, vertical weight-drops) are not applicable to Love-wave soundings. In fact, the only cost-effective sources for generating S_H-wave energy known to us are a sledge hammer with horizontal traction plank, Hasbrouck "golf shoe" source (Hasbrouck, 1983), or hammer-impact aluminum shear wave seismic source (Haines, 2007). Horizontal weight-drop or pendulum-type sources can be deployed to generate lower frequency energy but are time consuming to set up. Weight-drop sources that strike the ground at a 30º angle are more portable but need more testing. Large, horizontal Vibroseis™ energy sources are very well-suited for Love-wave testing but are very costly. Due to practical (such as source frequency limitations) and theoretical (such as lower frequency Love waves required to image to a specific depth than Rayleigh waves in many geologic conditions) considerations, active Love wave techniques are not particularly well suited to the imaging of V_S structure to 30-m depth at soft soil sites. Active Love wave techniques are better suited to the imaging of 30-m deep V_S structure at stiff soil and rock sites, where a sledge hammer and horizontal-traction plank source can generate sufficient energy over the required frequency range. Passive Love-wave techniques, however, can be useful for characterizing V_S structure of low-velocity sediment sites in urban environments.

2.2.2 Passive Surface-Wave Methods

Unlike active surface-wave techniques, the microtremor method records background noise emanating from ocean wave activity, atmospheric conditions, wind effects, traffic, industrial activity, construction activities, etc., and collectively are referred to as microseisms. Typically, microseisms with frequencies below 1 Hz have natural origins, whereas those with frequencies above 1 Hz are largely due to human activities (Okada, 2003). The most common techniques used for analysis of microtremor data include: the single-station Nakamura Method (Nakamura, 1989); *f-k* methods, such as beam-forming (Lacoss and others, 1969) and maximum-likelihood (Capon, 1969); and the spatial-autocorrelation (SPAC) method, which was originally based on work by Aki (1957). The SPAC method has since been extended and modified (Ling and Okada, 1993; Ohori and others, 2002; Cho and others, 2004) to permit the use of noncircular arrays, and is now collectively referred to as extended spatial autocorrelation (ESPAC or ESAC). Separately, Bettig and others (2001) developed a modified SPAC routine specifically optimized for random arrays.

2.2.2.1 Horizontal-to-Vertical Spectral Ratio (HVSR) Technique

The horizontal-to-vertical spectral ratio (HVSR) technique, also known as the Nakamura Method, was first introduced by Nogoshi and Igarashi (1971) and later revised by Nakamura (1989). This method utilizes single-station recordings of ambient vibrations (microtremor or noise) made with a three-component seismometer. In this method, the ratio of the Fourier amplitude spectra of the horizontal and vertical components is calculated to determine the frequency of the maximum HVSR response, commonly accepted as an approximation of the fundamental frequency (f_0) of the sediment column overlying bedrock (see Section 2.5.1). The same method, but applied to earthquake records, is also used to determine site frequency (Lermo and Chávez-García, 1994.

However, the HVSR technique, as applied during this investigation, was based only on microtremors.

2.2.2.2 Array Microtremor (AM) Technique

The array microtremor (AM) technique utilizes four or more receivers aligned in a 2-D array. Although any 2-D arrangement of receivers will suffice—including randomly placed receivers—triangular, circular, semi-circular, and L-shaped arrays are commonly used. Receivers typically consist of 1- to 4.5-Hz geophones, although very deep (> 200 m) soundings will necessitate the use of 5- to 20-s seismometers. The triangular array, which may consist of several embedded equilateral triangles, is often used, as it provides good results with a relatively small number of geophones (fig. 3). With this array, the length of the side of the outer triangle should be at least equal to the desired depth of investigation. The L-shaped array is useful at sites located at the corner of perpendicular intersecting roads. Typically, 20 or more records of noise data, each with duration of 30- to 60-s, are acquired to image V_S structure in the upper 100 m. Some data acquisition systems may allow continuous recording for the duration of the measurement. Imaging the velocity structure to greater depths requires a significantly longer recording duration. As previously mentioned (Section 2.2.2), AM data are typically reduced using various *f-k* or SPAC methods.

2.2.2.3 ReMi™ Technique

Refraction microtremor (ReMi™), also known as the passive MAS_RW technique, is a passive surface-wave technique developed by Louie (2001). The ReMi™ method differs from the more established array microtremor technique in that it uses a linear-receiver array rather than a 2-D array and assumes multi-directional noise sources. Linear-array passive surface-wave datasets also can be extracted from 2-D arrays, such as the L-, T-, or X-shaped arrays. Although 2-D arrays are much more robust than a linear array, there are often field conditions (sidewalk, alley, edge of a developed property) where only a linear array can be applied.

ReMi™ field procedures typically consist of laying out a linear array of 24 4.5-Hz geophones and recording 20 or more noise records of 30–60-s duration. These noise records are processed using the software package SeisOpt® ReMi™ version 2.0 developed by Optim™ Software and Data Services. This package is used to generate and combine the slowness (*p*) - frequency (*f*) transform of the noise records. In practice, the surface-wave dispersion curve is picked at the lower envelope (fig. 6 in Martin and others, 2006, and site report for CE.12076) of the surface-wave energy identified in the *p-f* spectrum. Because the lower envelope of the surface-wave energy is picked rather than the peak, the resulting dispersion curve is somewhat subjective, particularly when records are noisy.

Linear array passive surface-wave data can also be analyzed with ESAC routines, but as with the ReMi™ technique, results will only be accurate if there are multi-directional noise sources. Linear passive arrays are generally best suited for extending the depth of investigation of active surface-wave soundings in urban environments to a maximum depth on the order of 100 m. When using linear passive arrays to image V_S structure to depths greater than 100 m, the very low-frequency noise sources required are inherently more likely to have a directional noise bias.

2.2.3 Active and Passive Surface-Wave Modeling

Rayleigh and Love waves have multiple modes of propagation, which correspond to plane waves in 2-D space, when traveling in a vertically heterogeneous media. The SASW technique measures apparent-phase velocities (also referred to as effective- or average-phase velocities), which correspond to the superposed mode of fundamental and higher-mode surface waves, as well as the effects of body wave refraction/reflection. The phase velocities identified using MAS_RW or MAS_LW will correspond to either individual modes of surface-wave propagation, or an effective mode, depending upon the complexity of the velocity structure. Resolution in the wavenumber domain, which depends on the number of receivers and the array length, also affects the interpreted dispersion curve: a small number of receivers and a short array length results in poor phase velocity resolution, whereas a large number of receivers and a long array length improve resolution. In normally dispersive media, where V_S increases with depth, the apparent Rayleigh- and Love-wave phase velocities generally correspond to the fundamental mode. There are, however, some cases of normally dispersive velocity structure where dominant higher modes and, thereby, modal superposition may occur in Rayleigh-wave data. These include: sites with a relatively thin low-velocity layer above a layer of much higher velocity; sites with a steep velocity gradient; or, sites with an abrupt increase in V_S at depth. In the first case, higher-mode Rayleigh waves may have significantly higher amplitude than the fundamental mode over a wide frequency range. In the two latter cases, the fundamental-mode Rayleigh wave may jump to the first higher mode, or the fundamental and first higher modes may become superposed at low frequencies. At such sites, Love-wave techniques may be preferred because the fundamental-mode Love wave is expected to be dominant at all frequencies.

In inversely-dispersive (velocity decreases with depth) and irregularly-dispersive (interspersed high- and low-velocity layers) media, higher-mode Rayleigh and Love waves may be dominant over some frequency ranges. In this case, the apparent phase-velocity data from SASW surveys will likely consist of superposed modes. In some cases, MAS_RW or MAS_LW data may be able to resolve multiple modes, albeit accurate identification of the modes is not always straightforward. However, in many cases the phase-velocity dispersion curves derived from either MAS_RW or MAS_LW data will consist of superposed modes. Lu and Zhang (2006) presented a method for automatic identification of higher modes based on the relative amplitude of Rayleigh-wave modes. Strategies that have been developed to estimate the effective Rayleigh wave mode, neglecting body wave refraction and reflection, for active and passive surface-wave data assume far-field plane Rayleigh wave propagation only (Tokimatsu and others, 1992), or incorporate source and receiver geometry using strategies outlined in O'Neill (2003) or Lai and Rix (1998, 1999). The Kausel and Röesset (1981) 3-D array-based solution, which is used to numerically simulate the effective mode for a SASW survey, can account for source-receiver geometry and body wave effects. Tokimatsu and others (1992) provided a technique for estimating the effective mode for a two-station SASW procedure that incorporates source-receiver geometry, but does not include body-wave effects.

The forward problem is typically solved using the Thomson-Haskell transfer-matrix (Thomson, 1950; Haskell, 1953), dynamic stiffness matrix (Kausel and Roësset, 1981), or reflection and transmission coefficient (Kennett, 1974) methods. All these

methods can determine fundamental- and higher-mode phase velocities, which correspond to plane waves in 2-D space. The transfer-matrix method is often used in MAS_RW and passive surface-wave software packages, whereas the dynamic stiffness matrix is utilized in many SASW software packages. MAS_RW and/or passive surface-wave modeling may involve modeling of the fundamental mode, some form of effective mode, or multiple individual modes (multi-mode). As outlined in Roësset and others (1991), several options exist for forward modeling of SASW data. One formulation takes into account only plane Rayleigh-wave motion (called the 2-D solution), whereas another includes all stress waves and incorporates a generalized receiver geometry (3-D global solution) or actual receiver geometry (3-D array solution). The 2-D solution effectively models the fundamental mode but can account for approximate modal superposition that may occur at high frequencies, due to a either high-velocity surface layer or shallow high-velocity layer. The 3-D array solution is the most accurate method of modeling SASW data.

The particular technique preferred for modeling depends on the velocity structure, surface-wave methods used, resolution of the extracted phase-velocity data, and data reduction techniques. The fundamental mode is generally applicable to modeling Rayleigh-wave dispersion data collected at normally dispersive sites, providing there are not abrupt increases in velocity or steep velocity gradients; however, effective-mode or multi-mode approaches are often required for irregularly dispersive sites. If active and passive surface-wave data are combined, or MAS_RW data are combined, from multiple seismic records with different source offsets and receiver gathers, then effective-mode computations are limited to algorithms that assume far-field plane Rayleigh wave propagation. Linearized matrix inversion methods or global search methods (Monte Carlo approaches such as simulated annealing, generic algorithms and neighborhood algorithm) are typically used to solve the inverse problem.

It may not always be possible to develop a coherent, fundamental mode dispersion curve over sufficient frequency range for modeling from MAS_RW data due to dominant higher modes. Furthermore, higher modes may not be clearly identified for multi-mode modeling. It may, however, be possible to identify the Rayleigh-wave phase velocity of the fundamental mode at 40-m wavelength (V_{R40}), in which case V_{S30} can at least be estimated using the Brown and others (2000) relationship:

$$V_{S30} = 1.045 V_{R40,}$$

which was established based on statistical analysis of a large number of surface-wave datasets from sites with control by velocities measured in nearby boreholes.

There are little published data on the effects of lateral-velocity variation on the 1-D velocity structure assumption made for surface-wave modeling. There are several methods outlined for identifying lateral velocity variation in MAS_RW data such as multi-offset phase analysis (Strobbia and Foti, 2006) and another methodology developed by Boiero and Socco (2011). However, these schemes are best suited for Seismic-refraction surveys dentifying lateral-velocity variation beneath very long arrays, whereby, segments of the array satisfying the 1-D velocity structure assumption can be extracted for modeling. Seismic-refraction surveys may also be used to quantify lateral-velocity variation. Often, varying degrees of lateral variation occur beneath MASW arrays of the minimum length required to image to the desired depth of exploration. In such cases, use of only a small segment of the array for analysis is not an option. More research is needed

to assess the effects of common types of lateral-velocity variation (low-velocity surface layer of slightly variable thickness, shallow dip of velocity structure, undulating velocity structure, etc.) on V_S models derived from surface-wave dispersion curves. Such lateral-velocity variation causes significant scatter in the surface-wave dispersion data extracted from a MAS_RW or MAS_LW dataset. This scatter may be used to quantify lateral-velocity variation; either by modeling the upper and lower envelopes of the dispersion data in addition to the smoothed-average dispersion curve, using the scatter to assign error bars to the dispersion data and modeling using global inversion routines, or by using the variation of V_{R40} to estimate the variation of V_{S30}. While it is expected that reliable estimates of V_{S30} can be made if a coherent dispersion curve can be extracted from a MAS_RW dataset, the relationship of the V_S model to the 2-D V_S structure beneath the array may not be clear. In some cases, the short wavelength (high frequency) dispersion data may be selectively biased towards lower phase velocities associated with the sediments beneath a small segment of the array. In such cases, caution should be used when applying multi-mode or effective-mode modeling routines because lateral-velocity variation may be such that the fundamental mode was successfully recovered, while, the resulting 1-D V_S model would be expected to excite dominant higher modes over some frequency range.

The SASW and MASW techniques can generally be used interchangeably for characterizing the V_S structure in the upper 30 m, particularly at normally dispersive sites where V_S gradually increases with depth. SASW is the technique better suited for deep (40–100 m or greater) active surface-wave soundings because large energy sources, such as bulldozers or vibrators, can be more efficiently utilized. The SASW technique generally requires a shorter receiver array to image to a specific depth than the MAS_RW technique and may, therefore be better suited for characterizing sites with significant lateral velocity variation. However, the MAS_RW technique may be better suited for sites with complex velocity structure, such as inversely dispersive sites (near-surface velocities decrease with depth) or irregularly dispersive sites (velocity inversions, high velocity layers, etc.), because dominant higher-mode Rayleigh waves, if present, can be more readily identified. There are, however, SASW modeling routines (3-D global and array inversion) capable of addressing modal superposition and body-wave effects, which in some cases may be more easily implemented than effective- or multi-mode analysis of MAS_RW data. Complex wave propagation, associated with significant lateral-velocity variation and non-planar geologic structures can be clearly evident on MAS_RW seismic records but not in SASW data as only two to four receiver stations are typically utilized. MAS_RW seismic records can also be utilized for P-wave refraction analysis to identify the approximate depth and P-wave velocity (V_P) of the saturated zone. Anchoring the depth to the V_P of the saturated zone improves the accuracy of V_S models developed from the inversion of Rayleigh-wave dispersion curves.

Active and passive surface-wave techniques can be used as complementary techniques (table 3). For example, active surface-wave techniques, such as SASW, MAS_RW, and MAS_LW, image the shallow-velocity structure that cannot be accurately described by the passive AM techniques for estimating V_{S30}. AM techniques, however, work best in noisy environments where depth penetration by active techniques can be limited. In noisy environments, the AM technique can be used to extend the depth of V_S profiles derived from SASW, MAS_RW, and/or MAS_LW data. The degree of fit in the

overlapping portions of the dispersion curves from more than one technique increases the level of confidence in the final results.

As previously mentioned, the theoretical models used to interpret the surface-wave dispersion assume horizontally layered, laterally invariant, homogeneous-isotropic material, that is, subsurface structure with 1-D response. Although these conditions are seldom strictly met at a site, results from surface-wave surveys do provide a good "global" estimate of the material properties along the array hence may be more representative of the site than a borehole-based "point" estimate.

2.2.4 Active Body-Wave Methods

2.2.4.1 Seismic P- and S-Wave Refraction Techniques

Detailed discussions of the seismic-refraction method are provided in Redpath (1973), Dobrin and Savit (1988), and Telford and others (1990). Of two basic types, compressional (P) wave and shear (S) wave, P-wave surveys are more commonly conducted.

When conducting a refraction seismic survey, seismic waves are generated by an energy source such as a sledgehammer impacting a metallic plate (vertically for P-wave and horizontally for S-wave), a weight drop (horizontal, vertical or at an angle), vibratory source (vertical or horizontal), or an explosive charge. These seismic waves propagate into the subsurface at a velocity dependent on the elastic properties of the material through which they travel. When the waves reach an interface where the density or velocity changes significantly, a portion of the energy is reflected back to the surface and the remainder is transmitted into the lower layer. Where the velocity of the lower layer is higher than that of the upper layer, a portion of the energy is also critically refracted along the interface. Critically refracted waves travel along the interface at the velocity of the lower layer and continually refract energy back to the surface. Receivers (geophones) laid out in a linear array on the surface, record the incoming refracted and reflected waves. The seismic-refraction method involves analysis of the travel times of the first energy to arrive at the geophones. These first arrivals are from either the direct wave (at geophones close to the source), or critically refracted waves (at geophones further from the source). Where subsurface velocity structure is complex, converted waves may be erroneously interpreted as S-waves; therefore, it is important to validate S-wave refraction models with P-wave refraction models, at least when the saturated zone does not occur within the depth range of interest.

Analysis of seismic-refraction data depends on the complexity of the subsurface velocity structure. If the subsurface target is planar in nature, then the slope intercept method (Telford and others, 1990) can be used to model multiple horizontal or dipping planar layers. A minimum of one end-shot is required to model horizontal layers and reverse end-shots are required to model dipping planar layers. If the subsurface target is undulating (buried topography of a bedrock valley), then layer-based analysis routines such as the delay-time method (Wyrobek, 1956; Gardner, 1967), time-term inversion method (Scheidegger and Willmore, 1957), Hales method (Hales, 1958), plus-minus method (Hagedoorn, 1959), reciprocal method (Hawkins, 1961) (also referred to as the ABC method), wave-front method (Rockwell, 1967), and generalized reciprocal method (GRM) (Palmer, 1980) are required to model subsurface velocity structure. These

methods generally require a minimum of five shot-points per spread (end shots, off-end shots, and a center shot). If the subsurface velocity structure is complex and cannot be adequately modeled using layer-based modeling techniques because of complex weathering profile in bedrock, numerous lateral velocity variations, etc., then Monte Carlo or tomographic inversion techniques (Schuster and Quintus-Bosz, 1993; Zhang and Toksöz, 1998) are required to model the seismic-refraction data. These techniques require a high shot density, for example, at every two to six stations (geophones). Additionally, most tomographic inversion techniques cannot effectively take advantage of off-end shots to extend the depth of investigation, so longer profiles are required.

Velocity inversions, hidden layers, or lateral velocity variations can also cause errors in seismic-refraction models. A velocity inversion is a geologic layer with a lower seismic velocity than an overlying layer. Critical refraction does not occur along such a layer because velocity has to increase with depth for critical refraction to occur. This type of layer, therefore, cannot be recognized or modeled and depths to underlying layers will be overestimated. Velocity inversions may occasionally occur at soil sites and may be quite common at sedimentary rock sites, but are not expected in weathered crystalline rock. A hidden layer is a substrate where velocity increases, but does not give rise to a first arrival because it is of insufficient thickness relative to the contrast in velocity with the bounding layers. Because the seismic-refraction method generally only involves the interpretation of first arrivals, a hidden layer cannot be recognized or modeled, hence depths to underlying layers would be underestimated. A subsurface velocity structure that increases continually as a function of depth rather than as discrete layers will also cause depths to subsurface refractors to be underestimated, in a manner very similar to that of the hidden layer problem. Lateral velocity variations that are not adequately addressed in the seismic models will also lead to depth errors. Tomographic imaging techniques can often resolve the complex velocity structures associated with hidden layers, velocity gradients and lateral velocity variations. At sites with steeply dipping or highly irregular bedrock surfaces, or complex velocity structure, out of plane refractions (refractions from structures to the side of the line rather than from beneath the line) may add significant errors to the model.

2.3 Selection of Geophysical Techniques for Field Deployment and Site Characterization Strategies

The approach to deploying the aforementioned geophysical techniques was primarily based on: (1) the known capabilities of the standalone technique or methods (groups of techniques) as previously outlined; (2) map information and on-site reconnaissance for assessing the geologic and noise conditions at each station; and (3) lessons learned as the investigation progressed.

Stations were summarily categorized as rural (r), suburban (s), or urban (u) to account for noise conditions, and as soil or rock to estimate geologic conditions (table 3). Urban, and possibly suburban, sites were expected to have sufficient noise (energy) to apply passive surface-wave techniques. For the purpose of this project, shallow-rock sites were defined as soil sites with expected high-velocity sedimentary or crystalline rock at depths less than the exploration depth of the surface-wave techniques utilized. Rock sites were defined (using geologic maps) as being Tertiary or older sediments, sedimentary

rock or crystalline rock (volcanic, intrusive, and metamorphic) at or immediately beneath the surface.

The HVSR technique was used at all sites. HVSR measurements typically were made at three locations of each array for two main purposes: to demonstrate whether or not modeling the subsurface velocity structure as being 1-D is appropriate, and to estimate the fundamental resonance frequency of the site. The HVSR measurement locations were generally distributed at the end- and mid-points of each survey array segment. Frequently, one of the HVSR records was obtained adjacent to the seismographic station.

Rural soil sites were always characterized by the MAS_RW method. In addition, SASW techniques were often used at rural soil sites, particularly those that were expected to have relatively low V_S. The first arrival refraction data from the MAS_RW records were always reviewed to determine if the water table was located at shallow depth and, if so, the depth to and the P-wave velocity of the saturated zone was estimated. Occasionally, an inferred water table seismic reflector was used to estimate the water table depth.

Urban soil sites were typically characterized using the combination of MAS_RW, AM, and ReMi™ techniques. The MAS_RW technique was applied to characterize shallow velocity structure, whereas the AM and ReMi™ techniques ensured that a depth of investigation of at least 30 m was achieved. The 2-D AM geometries typically applied included a 7- or 10-channel triangular array with 1-Hz geophones and/or a 48-channel L-shaped array with 4.5 Hz geophones. The L-shaped array was most commonly deployed because there was insufficient space for the triangular arrays at most sites, for example, an L-shaped array could be deployed along property boundaries or at street intersections. Additionally, data from either or both of the two linear segments of the arrays could be later extracted from an L-shaped array for ReMi™ analysis. In this project, both 2-D and linear array passive surface-wave data were acquired at each site to compare results in a variety of noise conditions.

Shallow rock sites in rural environments were typically characterized using the MAS_RW technique, supplemented by P-wave seismic-refraction data. In urban environments, passive surface-wave data were also acquired in addition to the aforementioned methods. During the early phases of the investigation, it was recognized that the MAS_RW technique was not effective at some sites; in particular, sites where a thin sediment layer (about 10-m thick or less) overlying high-velocity rock excites dominant higher Rayleigh-wave modes at lower frequencies. Therefore, and although being outside the scope of work, attempts were made to characterize such sites using the S-wave seismic refraction and/or MAS_LW (Love wave) techniques. The MAS_LW technique was generally quite effective at sites with shallow rock. As depth to rock increased, Rayleigh-wave techniques were also effective; however, when interpreting Rayleigh-wave dispersion data, the possibility of mode jumping (fundamental to first higher mode) or modal superposition (mode mixing) had to be considered. Surface-wave techniques are not particularly well-suited for accurately characterizing the V_S of relative high velocity rock, even when rock is quite shallow (surface-wave wavelengths much longer than typically recorded are required to accurately constrain the V_S of shallow rock). Hence, S-wave seismic refraction was applied (whenever possible) to help constrain and validate the V_S of rock.

Rock sites were generally the most difficult sites to characterize due to limited accessibility, lateral velocity variation and occasional dominant higher mode surface waves. Topographic variation at rock sites often limited testing to a ridge top or toe of slope of an outcrop and occasionally required that testing be conducted further away from the seismic station than desired.

During the early phases of field investigation, lateral velocity variation was significant at many rock sites. Therefore, the P-wave seismic-refraction technique—anticipated for use only at about 30 to 40 percent of rock and shallow rock sites—was eventually used at almost all rock sites. Typically, P-wave seismic-refraction data were acquired concurrently with MAS_RW data by adding multiple interior shot locations along the MAS_RW array. These interior shot locations also proved useful for MAS_RW analysis at many sites, particularly those with significant lateral velocity variation or dominant higher modes at high frequencies. Occasionally, P-wave seismic-refraction data were acquired using longer arrays to image to the 30-m depth without the use of far-offset shot locations. In many cases, seismic-refraction models were used to quantify lateral velocity variation beneath the portion of the seismic line where the depth of investigation was greatest. However, this process was not initiated until a number of sites were encountered that required the use of seismic-refraction models to assess V_{S30} or validate surface wave V_S models. The P-wave refraction technique was not always effective at rock sites due to weak P-wave signals, out-of-plane refractors, scattering, etc.

When lateral velocity variation was too extreme, a coherent surface-wave dispersion curve could not be developed and surface-wave techniques were ruled ineffective. When a coherent dispersion curve could be developed for a site with significant lateral velocity variation, large scatter was observed in the dispersion data resulting in a V_S model that may not be representative of the average velocity structure. V_{S30}, however, likely falls within the range beneath the test area and is still useful for the purpose of site characterization. A small (5°) dip in velocity structure at depth can result in long wavelength divergence of surface-wave dispersion data reduced from forward and reverse source locations. Near-surface lateral velocity variation, which was very common, results in significant scatter in short wavelength dispersion data. Lateral velocity variation can also severely complicate attempts at multi-mode or effective-mode inversion, particularly if the short wavelength (high frequency) segment of the dispersion curve is biased to a portion of the array with lower V_S. Some rock sites had dominant higher Rayleigh-wave modes over a wide frequency range, often associated with a very thin low velocity residual soil layer over stiffer sediments or rock. The MAS_LW technique, which again was not within the original scope of work, was effectively used at many such sites. Additionally, rock sites with relatively abrupt increases in velocity at depth or steep velocity gradients (such as weathered crystalline rock sites) often include superposition of Rayleigh wave modes at long wavelengths (low frequencies). The MAS_LW technique was not typically applied to this type of site but should be considered for future investigations, as modal superposition or mode jumping is not expected to be an issue with Love wave dispersion data.

A number of seismic stations sited on rock were located at the toe of bedrock outcrops (mountain or hill). These sites could not generally be characterized with surface-wave methods, as the bedrock surface dips beneath an array aligned along the toe of slope. S-wave seismic-refraction surveys, which were not part of the original scope of

work, were conducted in an attempt to characterize such sites. S-wave seismic-refraction models were typically only included in the site reports if S-wave first arrivals could be reliably interpreted. Strong P-wave energy and converted waves were prevalent in some S-wave refraction datasets and limited the use of the data.

Other seismic stations were located on dipping sedimentary rock. Ideally in such conditions, the seismic arrays are aligned parallel to strike and also, when possible, perpendicular to strike to assess the variations in lateral velocity. However, local surface topography often limit ideal survey locations, hence it was not usually possible to place arrays parallel or perpendicular to strike while also minimizing topographic variation along the array. Often, dipping sedimentary rock sites had relatively low velocity, thereby behaving more like a soil site, or near-surface velocity was controlled predominately by weathering rather than lithology. Here, surface-wave techniques were relatively effective even when arrays were aligned at an oblique angle to strike of the geologic bedding.

2.4 Field Procedures

2.4.1 Survey Control

For control on the surveys, the end- and mid-points of each geophysical array were surveyed with a Magellan Professional MobileMapper™ CX GPS system or Trimble Pro XRS GPS system with OmniStar differential corrections. When accessible, the seismic station also was surveyed. The assigned datum for all coordinate values is the World Geodetic System 1984 (WGS84). Tree cover at several sites required geophysical arrays to be surveyed with a Nikon NPL-362 total-station surveying system and tied to GPS control points. All geophone and shot point locations were based on 100-m tape measure(s). Relative elevations of seismic-refraction lines were surveyed using a Sokkia C300 automatic level or total-station system.

2.4.2 HVSR

The primary seismic system used to acquire HVSR data was a Nanometrics Trillium Compact 120-s seismometer (herein referred to as Trillium Compact) and a Kinemetrics Quanterra Q330 data recorder (fig. 4). HVSR measurements were also made at some sites with a Micromed Tromino ENGY (herein referred to as Tromino) (fig. 4). A minimum of three HVSR recordings was made at each site. The measurement locations were either distributed along the measurement array(s), or often, one HVSR location was placed near the seismic station. The HVSR data acquisition procedures generally followed user guidelines developed under the Site EffectS assessment using Ambient Excitations (SESAME) research project (SESAME, 2004).

It was necessary to take an appreciable amount of time to determine the optimal method of deploying the Trillium Compact for HVSR measurements. The best quality data were generally acquired when the sensor was placed in a shallow hole and coupled to the ground by a small aluminum cradle with spikes, provided by the manufacturer. The sensor was always covered with a bucket or plastic tub to keep direct wind off the sensor and, more importantly, to keep the wind from moving the sensor cable. In gravelly soils, the sensor was placed in a small hole with the aluminum cradle coupled to the ground using gypsum plaster (plaster of Paris). On hard substrate, the sensor was either placed directly on the ground and coupled by leveling legs or was placed on the aluminum

cradle without legs. Microtremor (noise) data were recorded at a 200-Hz sample rate and output to 3 column ASCII files, each containing 1-hr blocks of data, with columns 1 through 3 comprised of the vertical, north, and east components, respectively. Typically, the Trillium Compact was set up and recording for at least 15 min (settling time) before other field activities were suspended for HVSR recording.

The Tromino is a higher frequency seismometer, optimally designed for HVSR measurements in shallow sedimentary basins. The Tromino was typically only used at sites expected to have relatively shallow bedrock. The Tromino was coupled to the ground using three spikes provided by the manufacturer or geophone spikes adapted for the instrument. Microtremor measurements were typically made for between 15 and 45 min, depending on site conditions, with data recorded at 128 samples per second. Recordings were stored in the instrument's internal memory, downloaded to a laptop computer, viewed in the software package (Grilla) provided by Micromed, and reformatted to an ASCII file for further analysis.

2.4.3 SASW

SASW equipment consisted of Oyo Geospace 1-Hz and 4.5-Hz geophones, a Hewlett Packard (HP 35670A) dynamic signal analyzer, hammers of various sizes, and a 90-kg accelerated weight drop (AWD) as shown in figure 5.

SASW data were generally acquired using a common-receiver-midpoint geometry, where the midpoint of the receivers remained fixed during data acquisition (fig. 5). An alternate acquisition geometry, which was not typically applied during this investigation, is the common-source geometry where the source location remains fixed during data acquisition. The common-source geometry is typically applied when large energy sources (Vibroseis^{TM}) that are inefficient to move are used.

SASW data typically were collected by spacing base receivers 2, 4, 8, 12, 16, 24, and 32 m apart; spacing of additional receivers were used as necessary. The spacing of receivers generally provided adequate overlap of dispersion data over a range of wavelengths between 1 and 64 m. For each receiver spacing, reversed source locations were occupied with a common-receiver midpoint, where possible. The distance between the source and near receiver was typically set equal to the receiver spacing. A rock hammer, a 3-lb hammer, 10- to 20-lb sledgehammers, and an AWD were used as energy sources—larger energy sources were used as receiver spacing increased. Data from the transient impacts (hammers) were averaged 10–20 times to improve the signal-to-noise ratio. Data were saved to floppy disk and file names and field parameters were documented.

2.4.4 MAS$_R$W and MAS$_L$W

The MAS$_R$W and MAS$_L$W seismic data acquisition system consisted of two 24-channel Geometrics Geode signal enhancement seismographs combined to form a 48-channel system and a laptop computer running the Geometrics Seismodule Controller. Equipment used for the MAS$_R$W surveys consisted of Geospace 4.5-Hz vertical geophones, seismic cable with 3 m-take-outs, a truck mounted AWD, a 3-lb hammer, 10- and 20-lb sledgehammers, an aluminum plate, Geometrics hammer switches and a trigger cable. Equipment for MAS$_L$W surveys consisted of Geospace 4.5 or 10-Hz horizontal geophones and a 10- or 20-lb sledgehammer with a horizontal traction plank (wood beam

with metallic cleats), Hasbrouck "golf shoe" source (Hasbrouck, 1983), or hammer-impact aluminum shear wave seismic source (Haines, 2007). Photographs of the aforementioned equipment are shown in figure 6.

Each MAS_RW array typically consisted of a single spread of 48 geophones, spaced 1.5 m apart. With this survey design, source locations were most commonly offset at 1.5, 5, 10, 20, and 30 m from the near geophone at each end of the array (fig. 6). Occasionally, the farthest offset shot locations were not included as a result of insufficient space. The basis of this survey design was to allow extraction of Rayleigh wave dispersion data to a sufficiently long wavelength to develop a 30-m deep V_S model, while abiding by the near-field criteria presented by Yoon and Rix (2009). At sites with a lack of sufficient space, 1-m geophone spacing was used. One-meter geophone spacing was also used at most sites where passive surface-wave data were acquired. Additionally, MASW data were occasionally acquired along longer arrays deployed to extend the seismic-refraction depth of investigation.

When permitted, the AWD was used as an energy source at all off-end shot locations; otherwise, a 20-lb sledgehammer was used as the primary source. However, most sites without vehicle access for the AWD had relatively high S-wave velocity, and therefore a 20-lb hammer was sufficient to image to 30-m depth. In low noise environments, the AWD and 20-lb hammer sources generally provided sufficient energy to about 4-5 and 7-8 Hz, respectively. Large vibratory energy sources are expected to perform better at low frequencies, but were not used during this investigation. A 3-lb hammer and light blows with a 10-lb hammer were also used near the shot location at 1.5-m offset from the near geophone in an attempt to generate higher frequency surface waves. Multiple energy sources were also used at a center shot location during standard MAS_RW data acquisition. At rock sites, seismic-refraction data were also acquired along MAS_RW arrays by adding interior shot locations at intervals of 4 to 6 geophones. The additional refraction shots often proved very useful for MAS_RW analysis at sites with significant lateral velocity variation. Seismic data were acquired with a record length of 1 s or longer and a 0.125 ms sample rate to allow both surface-wave and seismic-refraction analysis. Generally, the final seismic record at each shot point was the result of stacking 5–15 shots to increase the signal-to-noise ratio. Data were saved to an internal hard drive of a laptop computer. Data file names and important acquisition parameters were documented.

The design of the MAS_LW survey was similar to MAS_RW design. For this technique, 4.5- or 10-Hz horizontal geophones and a hammer and wooden traction plank with a vehicle as hold-down weight, or hammer and portable aluminum S-wave source, were used as energy sources. Lower frequency energy sources were not available for MAS_LW surveys, primarily because the technique was not originally part of the scope of work and was typically only applied at relative high velocity sites. MAS_LW data were generally acquired in conjunction with S-wave seismic-refraction data along the same array. Both forward and reverse polarity seismic records (hammer blows to opposite sides of the source) were acquired at each shot location.

2.4.5 AM and ReMi™

Four array configurations were used for acquisition of data from the array microtremor method (AM) (fig. 3):

- 7-channel triangular array with 1-Hz geophones
- 10-channel triangular array with 1-Hz, geophones
- 48-channel L-shaped array with 4.5-Hz geophones
- 48-channel T-shaped array with 4.5-Hz geophones

Triangular arrays typically have a minimum of four sensors: a sensor at each corner of an equilateral triangle and a sensor at the center of the triangle. In addition to the aforementioned geometry, the 7-channel triangular array has a smaller triangle array rotated 180° and embedded within the outer triangle with a maximum dimension of half the outer triangle (fig. 3). In the case of the 10-channel triangular array, a third triangular array is embedded in the inner triangle. The maximum length of the sides of the triangular arrays used in this project ranges from 50 to 80 m. L- and T-shaped arrays typically had 24 geophones on each leg of the array, with geophone spacing varying between 3 and 7.5 m. In order to verify that, under some noise conditions, passive surface-wave data at frequencies lower than 4.5 Hz can be extracted from arrays using 4.5-Hz geophones, a 9-channel L-shaped array was co-located with a 48-channel L-shaped array at one site (CE.14395).

ReMi™ data was also collected at all sites where passive surface-wave measurements were made in order to compare dispersion data extracted from linear arrays to that extracted from the 2-D arrays. Passive ReMi™ data were either acquired along a separate array (at sites where triangular arrays were utilized) or extracted from 48 channel "L" or "T" array datasets.

A Geometrics Geode 24-channel seismic-recording system was used to record the passive surface-wave data. Data were typically acquired during HVSR recordings when there was sufficient time to record 30–50 30-s records. Data were stored on a laptop computer and data acquisition parameters, array geometry and file names were documented.

2.4.6 P- and S-wave Seismic Refraction

Both the data acquisition system and the seismic sources used for the seismic-refraction surveys are the same as those used for the MAS_RW and MASLW surveys (Section 2.4.4). Similarly, the P-wave refraction surveys utilized 4.5-Hz vertical geophones, but for the S-wave surveys, 4.5-, 10-, and 28-Hz geophones were used.

Each seismic line consisted of a single spread of 24 or 48 geophones spaced 1.5–3 m apart. Seismic-refraction data were generally acquired in conjunction with MAS_RW or MAS_LW data from arrays with 1.5-m geophone spacing. About 15–23 seismic-refraction shot-point locations were occupied on each line: multiple off-end shots where necessary and possible, end shots and multiple interior shot-points were nominally located between every fourth or sixth geophone.

The AWD and 20-lb sledgehammer were typically used as energy sources for P-wave seismic-refraction data acquisition. A wooden traction plank or aluminum source was typically used for S-wave seismic-refraction data acquisition. Both forward and reverse (hammer blows to opposite sides of the source) polarity seismic records were acquired at each S-wave refraction shot location. Generally, the final seismic record at each shot point was the result of stacking 5–15 shots to increase the signal-to-noise ratio. Data were saved to computer with data file names and important acquisition parameters were documented.

2.5 Data Reduction and Modeling

2.5.1 HVSR Analysis

HVSR data were reduced using the Geopsy Version 2.7.0 software package (*http://www.geopsy.org;* last accessed June 27, 2012) developed by Marc Wathelet for the SESAME project. In Geopsy, the reduction of HVSR data generally adheres to the H/V user guidelines developed under the SESAME project (SESAME, 2004).

Microtremor data recorded by the Trillium Compact seismometer and Q330 data recorder were stored in files containing 1-h blocks of data. These data files were appended into a single file containing the vertical, north, and east components of recorded noise data, respectively. Although not necessary for HVSR analysis, the data were converted from counts to velocity units. Microtremor data recorded by the Tromino® were exported to an ASCII file using the software package Grilla, provided with the instrument. Upon export, a 0.3-Hz low-cut filter was automatically applied. Data files were then loaded into the Geopsy software package, where data file columns containing the vertical and horizontal (north and east) components and sample rate (200 Hz for Trillium Compact and 128 Hz for Tromino®) were specified. HVSR was typically calculated over a frequency range dependent on the observed site response and using a time window length of 100–200 s. Time windows containing transients (nearby foot or vehicular traffic) or segments yielding poor quality results were not utilized for analysis. Time windows were either: automatically picked and then manually edited; or, had an anti-triggering algorithm applied to avoid transients. For every selected time window, Fourier amplitude spectra were calculated and smoothed by the Konno and Ohmachi (1998) filter with a smoothing coefficient value between 30 and 40. The vertical amplitude spectra were divided by the root-mean-square (RMS) of the horizontal amplitude spectra to calculate the HVSR for each time window and the average HVSR. After calculating the standard deviation of the HVSR amplitudes for all windows, the average response is divided and multiplied by the standard deviation to produce the minimum and maximum HVSR spectra, respectively (SESAME, 2004).

Because HVSR measurements were primarily used to verify that a site's velocity structure was generally 1-D in nature and to determine the approximate fundamental resonance frequency, HVSR data were not generally modeled and no attempt was made to jointly invert HVSR and surface-wave dispersion data. Occasionally, and particularly for shallow rock sites, the HVSR modeling routines available in the software packages Grilla v. 6.1 (Micromed) and SeisImager/SW (Geometrics, Inc.) were used to calculate the theoretical HVSR response for the V_S models developed by inversion of the surface-wave dispersion data, and then these responses were compared to the measured HVSR data. The quarter-wavelength approximation method, first introduced by Joyner and others (1981) and adapted (Boore and Brown, 1998; Ibs-von Seth and Wohlenberg, 1999; Delgado and others, 2000) as:

$$f_0 = \frac{\overline{V}_S}{4z}$$

where f_0 is the site fundamental frequency, $\overline{V}_S$ is the average shear-wave velocity of the soil column overlying bedrock at depth z, was also used on occasion to determine if the

V_S model developed from the surface-wave dispersion data for shallow rock sites was consistent with the HVSR data.

2.5.2 Active and Passive Surface-Wave Analyses

Several software packages were used for reduction and modeling of active and passive surface-wave data. These commercial software packages included:

- Geometrics/Oyo Corporation SeisImager/SW v. 4.305—active and passive surface-wave reduction and analysis including fundamental-, effective- and multi-mode Rayleigh-wave inversion and fundamental-mode Love-wave inversion.
- Geogiga Seismic Pro 6.1 or Pro 7.1 Surface Plus and Surface—active and passive surface-wave reduction and analysis (fundamental-mode and multi-mode Rayleigh-wave inversion).
- Kansas Geological Survey SurfSeis 3—surface-wave analysis (fundamental- and multi-mode Rayleigh-wave inversion).
- SeisOpt ReMi™ v. 5.0 by Optim™ Software and Data Solutions (reduction and analysis of linear array passive surface-wave data).
- WinSASW v. 1.23 written by Sung-Ho Joh, University of Texas at Austin—SASW data reduction and viewing of surface-wave dispersion data.
- WinSASW v. 3.1.2 and v. 3.2.6 written by Sung-Ho Joh (Soil Dynamics Lab, Chung-Ang University, Korea)—SASW data reduction and modeling, generation of representative dispersion curve and fundamental-mode (2-D solution) Rayleigh-wave inversion and effective-mode (3D-global and 3D-array solutions) inversion of Rayleigh-wave dispersion data acquired using SASW method.

2.5.2.1 SASW Data Reduction

SASW data were reduced using the WinSASW software packages as follows:

- Input forward- and reverse-direction phase spectrum and coherence for a particular receiver spacing.
- Enter receiver spacing, geometry, and wavelength restrictions (maximum wavelength typically set to twice the receiver spacing).
- Mask phase data (either the forward and reverse directions individually or the average).
- Generate dispersion curve.
- Repeat for all receiver spacings and merge all dispersion curves.
- Document workflow and output files in spreadsheet.

2.5.2.2 MAS_RW and MAS_LW Data Reduction

MAS_RW and MAS_LW data were reduced using the Geogiga Surface Plus software package as follows:

- Input all seismic records into software.
- Enter receiver spacing, geometry, and wavelength restrictions, as necessary.
- Select receiver offset range for processing and mute noise at late times.
- Apply wavefield transform to seismic record to convert data to phase velocity—frequency space.

- Identify and pick dispersion curve (fundamental mode and/or effective mode).
- Repeat for all shot records and various receiver offset ranges.
- Enter all input and output data file names, shot locations, receiver geometry, and receiver-offset range into spreadsheet and calculate maximum wavelength by which to minimize near-field effects.
- Apply maximum wavelength criteria, reformat, and merge all data files.
- Load merged dispersion curve into WinSASW software package, review scatter in dispersion data, delete outliers and save final dispersion data for modeling.

MAS_RW and MAS_LW data-reduction strategies evolved as challenging datasets were encountered. MAS_RW data collected at soil sites typically involved the acquisition of multiple off-end and mid-point shot locations. Multiple energy sources (3-lb hammer, 10-lb hammer, 20-lb hammer, and/or AWD) were used at off-end and center-shot locations. Generally, no single seismic record yielded a dispersion curve covering a sufficient range of wavelength (or frequency) to develop a V_S model to a depth of 30 m with acceptable accuracy. It was, therefore, necessary to acquire dispersion data using multiple-source locations, source types, and different receiver gathers. As an example, to obtain short-wavelength (high-frequency) dispersion data, it was not uncommon to apply the wavefield transform to receiver gathers consisting of only the nearest 6 to 12 geophones when the energy source consisted of a 3-lb hammer. Occasionally, SASW analysis was applied to selected receiver pairs from MAS_RW seismic records to obtain shorter wavelength dispersion data or to supplement MAS_RW dispersion data at complex sites.

At rock sites, the multiple interior source locations that were acquired to complete a seismic-refraction survey were also available for surface-wave analysis. Lateral velocity variation was the single largest problem when characterizing rock sites. Variations of 20 percent or more in the average V_P of the upper 30 m (V_{P30}) were often observed over relatively short distances in seismic-refraction models at such sites. When lateral velocity variation was too severe, it was not possible to develop a coherent composite dispersion curve over a sufficient range of wavelengths for modeling. When it is possible to develop a coherent composite dispersion curve, it is often assumed that the resulting V_S model, or at least the estimate of $V_{S30,}$ is representative of average site conditions. The degree of scatter in the dispersion data may be useful for assessing lateral velocity variation. It, however, could be used to quantitatively assign errors bars whenever a global inversion routine was used to thoroughly search the model space. Nevertheless, we did not apply global inversion routines for inversion of the surface-wave dispersion curves during this project. At more complex sites, it was not unusual for the composite dispersion curve to be comprised of more than 100 dispersion curves derived from multiple shot locations and different receiver gathers. Little is published on the effects of lateral velocity variation on the V_S models and V_{S30} estimates developed from various surface-wave testing configurations. Information is also scarce on the effect of lateral velocity variation on the amplitude of higher modes. It is possible that certain types of lateral velocity variation may severely limit the application of effective- and multi-mode surface-wave modeling techniques.

The Rayleigh wave dispersion curves were generally assumed to associate with the fundamental or effective mode. Sites with large increases in velocity at relatively

shallow depth or steep velocity gradients were often observed to have a jump from the fundamental first higher Rayleigh mode at intermediate to low frequencies. For sites with dominant higher Rayleigh-wave modes at intermediate to high frequencies (except for sites with a high velocity surface layer), it was often possible to take advantage of the dependence of source offset on the amplitude of the higher modes to extract the fundamental-mode data over a wide range of frequencies. In some cases, lateral velocity variation was such that it was likely that the fundamental mode was recovered, albeit with significant scatter, even though dominant higher modes were expected. The selective picking of dispersion data to avoid obvious higher modes and the large number of dispersion curves from multiple shot offsets and receiver gathers limited the use of effective-mode routines that incorporate source offset or source and receiver geometry. Therefore, whenever potential modal superposition or mode jumping at long wavelengths (low frequencies) were observed, only effective-mode routines based on far-field Rayleigh-wave propagation were considered for modeling. The fundamental Love-wave mode appeared to be dominant on all MAS_LW datasets used for site characterization.

2.5.2.3 AM and ReMi™ Data Reduction

AM data, including 2-D and linear-array data, were reduced using the extended-spatial-autocorrelation (ESPAC or ESAC) routines in software application programs such as SeisImager/SW and/or Geogiga Surface Plus through the following steps:

- Input all seismic records into software.
- Enter receiver spacing, geometry, and wavelength restrictions, as necessary.
- Calculate the SPAC function for each seismic record and average.
- For each frequency calculate the degree of fit of a first-order Bessel function to the SPAC function for a multitude of phase velocities.
- Identify and pick dispersion curve as the best fit of the Bessel function for each frequency.
- Convert dispersion curves to WinSASW format for modeling with maximum wavelength typically set to about twice the average length of the sides of the 2-D array or the length of the linear array.
- Document input and output data files and critical analysis steps in a spreadsheet.

Passive ReMi™ data were reduced using the SeisOpt® ReMi™ data analysis package. Data reduction steps included the following:

- Extract linear arrays from L- and T- shaped arrays using the computer program seg2_edit (Ellefsen, 2003).
- Convert SEG-2 format field files to SEG-Y format.
- Preprocess data, including trace-equalization gaining and DC offset removal.
- Erase receiver geometry present in the file header.
- Compute the velocity spectrum of each record by *p-f* transformation.
- Combine the individual *p-f* transforms into one image.
- Pick and save the velocity spectrum image.
- Convert dispersion curve to WinSASW format with maximum wavelength typically set to the length of the array.
- Document input and output data files and critical analysis steps to spreadsheet.

Under optimal conditions, AM and ReMi^{TM} data originating from the same array typically yielded similar dispersion curves. In cases where data differed, the AM data were assumed to be most representative of site conditions, assuming all datasets agreed with the MAS$_R$W data over the frequency range where the dispersion data overlapped. There was, however, at least one site (CI.SBC) where lateral velocity variation was the source of the difference between dispersion curves obtained by the two methods. In this case, the ReMi^{TM} array co-located with the MAS$_R$W array yielded dispersion data that best agreed with the MAS$_R$W dispersion data.

2.5.2.4 Active and Passive Surface-Wave Data Modeling (V_S Profile and V_{S30} Value)

Prior to data modeling, it is necessary to develop a regularly sampled representative dispersion curve. Numerous schemes exist for generating a representative dispersion curve including manual picking, direct averaging, and more sophisticated averaging schemes. The moving average-curve fitting routine outlined in Joh (1996) (implemented in WinSASW v. 3.1.2) was used to generate representative dispersion curves for the SASW, MAS$_R$W, MAS$_L$W, and passive surface-wave datasets. These representative dispersion curves were typically sampled at equal logarithmic wavelength increments. When multiple surface-wave datasets were acquired at a site, individual representative dispersion curves were combined (weighted average) and resampled yielding a final representative dispersion curve for the combined dataset. Occasionally, lateral velocity variation was such that there was significant scatter in the dispersion data from co-located SASW and MAS$_R$W arrays, or from the forward- and reverse-source locations of an MAS$_R$W array. In such cases, it was common to develop independent representative dispersion curves for the SASW and MAS$_R$W datasets or two representative dispersion curves for the MAS$_R$W dataset.

Rayleigh-wave dispersion data (SASW, MAS$_R$W, AM, and ReMi^{TM}) were typically modeled using the 2-D solution in the WinSASW software program or effective (average) Rayleigh-wave mode routine in SeisImager/SW. The use of the multi-mode modeling routines available in SeisImager/SW, Surfeis 3, and Geogiga Surface/Surface Plus were explored in several datasets. In some datasets, the effective-mode solution in SeisImager/SW was often successful at modeling jumps from fundamental mode to first-higher mode at low frequencies without the need to use a multi-mode modeling routine. Love-wave dispersion data (MAS$_L$W) were modeled using the fundamental mode Love-wave solution available in SeisImager/SW.

All software packages used for analysis of the surface-wave dispersion data utilize linear inversion routines and require starting models. Typically, layer thickness was manually defined such that the first layer was no thinner than one-third to one-half the minimum wavelength with layer thicknesses generally increasing with depth. At some sites, seismic-refraction models were used to support an upper-layer thickness that was less than would be normally estimated based on the minimum wavelength.

Mass density was assumed in the models and allowed to increase with increasing velocity. Where V_P exceeded about 1,500 m/s, assumed density was loosely tied to the Nafe-Drake empirical relationship between V_P and density for saturated sediments and sedimentary rocks (Ludwig and others, 1970). Within the normal range encountered in geotechnical engineering, variation in mass density has a very small effect on surface-

wave dispersion. During Rayleigh-wave data modeling, the V_P of unsaturated soils and rock was most commonly estimated using a Poisson's ratio (v) of 0.3 and the following relationship (Sheriff, 2002):

$$V_P = V_S \sqrt{\frac{2(1-v)}{1-2v}} .$$

The V_P of the saturated zone—the depth of which was typically estimated from seismic refraction first arrival data or occasional identification of a possible water table reflector—was set to greater than 1,500 m/s or the actual velocity generally estimated from seismic-refraction data. Poisson's ratio is not required as an input parameter for inversion of Love-wave dispersion data.

Depending on the inversion routine utilized, a starting model was either developed based on the methodology outlined in Joh (1996) (Rayleigh wave only), defined by the user based on general characteristics of the dispersion curve and through several iterations of forward modeling (Rayleigh and Love wave), or estimated by mapping $\lambda/3$ (λ is wavelength) to depth and the following relationship (Rayleigh wave only):

$$V_S = 1.1 V_R .$$

Starting models were modified (whenever necessary) throughout the inversion process to improve the fit between the calculated and experimental dispersion curves.

Most dispersion curves were modeled based on the fundamental-mode assumption (2-D solution in WinSASW for Rayleigh wave and SeisImager/SW for Love wave). In some cases, superposition of the Rayleigh fundamental and first-higher modes was suspected at low frequencies due to steep velocity gradients or abrupt increases in velocity at depth. At some sites, insufficient resolution in the wavenumber domain associated with relatively high velocities and inadequate array length also may have contributed to apparent modal superposition in the Rayleigh-wave dispersion data. In these cases, the far-field effective-mode (generally referred to as average-mode in the data reports) solution in SeisImager/SW was used in an attempt to more accurately constrain V_S at depth, and in particular, the velocity of the half-space. At several sites, there was a strong possibility that the Rayleigh fundamental mode jumped to the first higher mode at intermediate to low frequencies due to a significant increase in V_S at depth. The effective mode solution in SeisImager/SW and 3-D global solution in WinSASW v. 3.1.2 (not applicable to MASW and passive SW data) often adequately estimated the mode jump without having to resort to multi-mode modeling routines. Effective-mode and fundamental-mode V_S models were often compared to seismic-refraction models to determine which model was most likely representative of the subsurface velocity structure. Effective-mode modeling was avoided in many cases when a wide wavelength or frequency range of the dispersion curve was affected by the effective-mode assumption because (when possible) the fundamental mode was specifically targeted at higher frequencies during data reduction.

V_S models resulting from inversion of the surface-wave dispersion data should be considered to be a representative rather than an accurate velocity profile due to the non-uniqueness inherent in any inversion process. Global inversion routines, which generate an ensemble of velocity models fitting the dispersion curve, were not used in this project.

In some cases, several V_S-versus-depth models were developed by perturbing the starting model (layer thickness and/or V_S) to demonstrate non-uniqueness (model equivalence) of the solution and the insensitivity of V_{S30} to model equivalence. At some sites with significant scatter in the dispersion data, both the upper and lower envelopes of the dispersion data were modeled to determine the approximate variation in V_S and V_{S30}.

Plots of the composite-experimental dispersion data, representative-dispersion curve and theoretical-dispersion curves, and associated V_S-versus-depth models resulting from inverse modeling of the dispersion data were developed for each site. Depth of investigation was typically assumed to be less than one-half of the maximum Rayleigh-wave wavelength and less than one-third of the maximum Love-wave wavelength. Typically, the dispersion data were presented as plots of the log of wavelength versus phase velocity rather than the more conventional frequency versus phase velocity. Wavelength is critical to the data modeling process and is too often not considered. For example, minimum wavelength is used to determine the minimum thickness of the surface layer (one-third to one-half the minimum wavelength) and depth of investigation (one-half to one-third the maximum wavelength). Additionally, criteria applied to minimize near-field effects will determine the maximum wavelength based on survey design. Review of data in wavelength-phase velocity space can be useful for designing the layering in the initial model rather than relying on automatic layer generation routines, which can over parameterize the inversion. Finally, a logarithmic wavelength sampling of the dispersion curve gives sufficient weight to the segment of the dispersion curve associated with deeper sediments. Linear-frequency sampling of the dispersion curve gives too much weight to near surface velocity structure. Log of frequency, equal period and other alternative sampling routines may also be viable.

Based on the model of the V_S profile developed for each station, the resultant V_{S30} value, defined as the ratio of 30 m to the shear-wave travel-time, is calculated by the following relationship (Boore, 2006):

$$V_{S30} = \frac{30}{\sum_i \Delta t_i}$$

where, the travel-time, Δt_i, is defined as the ratio of the depth interval, Δz_i, to the shear-wave velocity of the interval, $(V_S)_i$:

$$\Delta t_i = \Delta z_i / (V_S)_i \, .$$

In most seismographic networks, SM sensors are typically installed at the ground level; hence, the depth intervals (Δz_i) for these sites represent layers as measured from the ground surface to the 30-m depth. At CI network stations, however, sensors are housed inside insulated vaults, which are commonly buried 1–3 m below the surface. To account for the actual emplacement depths of these sensors, an adjusted V_{S30} value is calculated for each station and denoted as $V_{S(Z,\, Z+30)}$, where Z is the reference location in the V_S profile representing the emplacement depth and where the 30-m interval is determined. Using the same V_{S30} (Boore, 2006) relation and Z values reported by the network, $V_{S(Z,\, Z+30)}$ values are (instead) calculated using depth intervals estimated from the reported emplacement depths ($Z > 0$ m) to the 30-m depth ($Z + 30$) in each model of the V_S profile.

Occasionally, alternative strategies, as outlined in the site reports, were utilized to adjust V_{S30} to the inferred properties beneath the seismic station.

2.5.3 Seismic Refraction Data Modeling

Seismic-refraction data were typically modeled using the tomographic analysis technique available in the SeisImager™/2D software package developed by Oyo Corporation/Geometrics, Inc. Refraction tomography techniques are often capable of resolving complex velocity structures (velocity gradients) that were observed in bedrock weathering profiles. Layer-based modeling techniques, such as the GRM, or time-term method, were incapable of accurately modeling the velocity gradients that often occurred in weathered bedrock. The GRM method, as implemented in the software package Seismic Pro 6.1 Refractor (Geogiga, Inc.) was, however, used to model seismic-refraction data at several shallow bedrock sites.

The first step in data processing is picking the arrival time of the first energy received at each geophone (first-arrival) for each shot point. The first arrivals on each seismic record are either a direct arrival from a compressional (P) or shear (S) wave traveling in the uppermost layer, or a refracted arrival from a subsurface interface where there is an abrupt increase in velocity. First arrival times were selected using the automatic- and manual-picking routines in the software package SeisImager™/2D. These first-arrival times were saved in an ASCII file containing shot location, geophone locations, and associated first-arrival time. Uncertainty in the first-arrival times generally increases with distance from the shot point. S-wave seismic-refraction records from normal and reverse polarity shots were combined into a single seismic record for the picking of first-arrival data. An S-wave stack (reverse-polarity record subtracted from normal-polarity record to enhance S-wave energy and cancel P-wave energy) was also applied to facilitate picking of the S-wave first-arrival data.

Data quality was affected by factors such as: wind, surface conditions, traffic noise, and geologic conditions. No attempt was made to interpret seismic-refraction data when it was believed that a reliable interpretation could not be made due to noise or other factors (it was often much more difficult to pick S-wave seismic-refraction first-arrival data than P-wave first-arrival data due to P-wave interference, poor polarity reversal, potential converted waves). P-wave energy does not generally exhibit polarity reversal and could often be eliminated (to a certain extent) by using an S-wave stack. When clear reversed S-wave waveforms were not observed on normal- and reverse-polarity seismic records, error can be significantly larger in the first arrival data. At sites with complex velocity structure or even shallow dipping velocity structure, converted waves, which can exhibit polarity reversal, can occur as first-arrivals resulting in significant error in the S-wave velocity model. However, very high quality S-wave refraction data were generally acquired at sites where the velocity structure is generally 1D. Unless shallow rock or sediments were saturated, S-wave seismic-refraction models were typically correlated to P-wave seismic-refraction models to confirm that converted waves or first arrival picking errors did not seriously degrade the velocity model.

GRM was only applied to selected shallow bedrock sites, primarily to model the depth to, and seismic velocity of, the bedrock unit. First-arrival and elevation data were entered into the software package Seismic Pro 6.1 Refractor where time-distance plots for the forward- and reverse-shots were generated. Forward-shots were shot-points where

energy travels from geophone 1–48. Energy travels in the opposite direction for reverse- and interior-shots that have both forward and reverse components. The first-arrival data for all shot-points were then assigned to the layer from which they were refracted. Typically, two to three layers were assigned to the travel-time data. The travel-time data associated with the lower layers were then shifted (in time) to line up with the travel-time data associated with the zero-offset end-shot, thereby forming a single travel-time curve for each refractor along the line. This method was used for both forward- and reverse-shots according to the procedures outlined in Lankston and Lankston (1986) and Redpath (1973). GRM analysis was then conducted to develop a velocity model.

Almost all seismic-refraction data were modeled using the tomographic inversion routines available in SeisImager™/2D. After loading the seismic-refraction first-arrival and elevation data into the software package, travel-time data were inspected to determine if the velocity structure was consistent with a layered or smooth velocity gradient earth model. When the velocity structure appeared to exhibit layering, a simple two- to three-layer velocity model was developed using the time-term method (Scheidegger and Willmore, 1957) and used as the starting model for the tomographic inversion. If the velocity structure appeared to be exhibiting smooth velocity gradients, then a smooth velocity gradient starting model with 20 layers was generated by inserting parametric information such as the velocity of the top layer, maximum velocity at a user defined depth, and depth to the bottom of the model. Velocity models were generally extended to far-offset shot locations to increase the depth of investigation. A longer geophone array without far-offset shot locations is preferred for tomographic inversion of seismic-refraction data. However, for the purpose of efficiency, seismic-refraction data were generally acquired in conjunction with MAS_RW/MAS_LW data along the 70.5-m-long arrays with maximum source-offset of 30 m. At selected sites, seismic refraction was acquired along longer arrays with lengths up to 141 m to extend the depth of investigation. A minimum of 20–50 iterations of non-linear ray-path inversions was implemented to develop a velocity model with acceptable RMS error between the observed and calculated travel-time data. Tomographic inversion techniques will model a smooth velocity gradient even if a sharp-velocity boundary exists, particularly when a smooth-velocity gradient starting-model is used. The use of layered starting models can result in sharper velocity gradients over geologic contacts. Final tomographic velocity models for each seismic line were exported as ASCII files and imported into Surfer® v. 9, developed by Golden Software, where the velocity models were gridded, contoured and annotated for presentation.

At some sites, the seismic-refraction velocity models were analyzed to quantify lateral velocity variation beneath the array and to determine if a surface-wave V_S model is consistent with the P- or S-wave velocity structure. In the case of a P-wave seismic-refraction model, the segment of the model from the central portion of the line with the greatest depth of investigation was loaded into a Microsoft® Excel Spreadsheet developed for analysis. V_{P30}, the average V_P of the upper 30 m, was estimated along this interval by projecting the velocity at the base of the model to 30-m depth. The variation in V_{P30} along the central portion of the line provided an estimate of the degree of lateral velocity variation beneath the line. An average V_P model was developed over the central portion of the line by horizontally averaging the traveltime of each model cell and cell thickness, whereby the average V_{P30} for the central portion of the line could be determined. The V_P

model was converted to a V_S model for various realistic constant values of Poisson's ratio. A similar analysis was applied to S-wave seismic-refraction models for more direct comparison to the surface-wave V_S model.

A number of sites, typically seismic stations located at the toe of a bedrock outcrop, could only be characterized using S-wave seismic-refraction models, and one or two sites could only be characterized using P-wave seismic-refraction models. At other sites, V_S models and V_{S30} estimates from S-wave refraction models or estimated from P-wave refraction models—based on assumed constant Poisson's ratio—were used to corroborate surface-wave V_S models, particularly at sites with significant lateral velocity variation.

Complete seismic-refraction surveys were not typically conducted at soil sites; however, the reversed off-end and center-shot locations used for $MASW$ data acquisition provided sufficient seismic-refraction data for simple horizontal layer-based analysis. Seismic-refraction analytic utilities available in SeisImager™/2D and Geogiga SS Imager were used to interactively fit horizontal layer-based models to the seismic-refraction records to approximate P-wave velocity structure. The primary purpose of the refraction analysis was to estimate the depth to the water table and P-wave velocity of the saturated zone because constraining the saturated zone when modeling Rayleigh-wave dispersion data improves the accuracy of the resulting V_S model. At several sites, it was possible to estimate the depth of the saturated zone by analyzing a possible water-table reflector.

3.0 Results

At the end of this project, V_S profiles and V_{S30} estimates were produced for 187 stations in California and 4 in the CEUS (fig. 1). These results represent a significant increase (approximately doubling) in the number of measurement-based V_{S30} values for SM stations in California (Chiou and others, 2008; Yong and others, 2012). As a pilot project, the experience provided the Advanced National Seismic System with information necessary to begin evaluating measurement techniques and to develop guidelines for characterizing site conditions at other SM stations. Detailed geotechnical information specific to each station is provided as individual site reports in appendix A. The repository for raw data is linked to each report and can be accessed by double clicking the title (network-code.station-code) of each report. Another link to simultaneously download all site reports and raw data can be found on the U.S. Geological Survey Publications webpage describing this report (*http://pubs.usgs.gov/of/2013/1102/*). The following is an overview of results from this project.

Table 3 summarizes the stations included in this study by distinguishing each station through the combination of its network and station codes. This scheme serves as a unique identifier of each station in subsequent discussions and in the accompanying data reports (see appendix A). Following the station coordinates (provided by the respective network operators) are the abbreviations (see footnotes for definitions in table 3) of the type(s) of techniques (standalone or combination of techniques) used near each station, the site coordinates of the measurement array(s), and the maximum calculated distance (m) based on the coordinates of the station and of the measurement array(s). Next, estimates of V_{S30} and the adjusted V_{S30} (denoted as $V_{S(Z,\ Z+30)}$, unless an alternative approach was applied; see Section 2.5.2.4 and fig. 9), as well as the method(s) (using the

same abbreviation scheme) that are the basis for determining V_S models and V_{S30} values are provided. Other attributes of table 3 include the National Earthquake Hazards Reduction Program (NEHRP) and Geomatrix 3-letter (GMX) Site Classes as defined by the Building Seismic Safety Council (BSSC, 2003) and described by Chiou and others (2008), respectively. Noise, geologic, and lithologic conditions provide additional site information, which were mostly used for logistics when preparing for fieldwork.

To demonstrate that our measurement locations meet the Borcherdt (2002) recommendation of 300 m or less, the coordinates of the measurement array are defined as the farthest endpoint of the array from the station location. Most (84 percent) of the measurement arrays fall within the preferred 150-m radius; of these, six sites are at (CI.JEM) or significantly close (CE.13922, CI.CIA, CI.FHO, CI.CGO, and CI.IDO) to this limit. Twenty-seven sites (14 percent) are in the 150- and 300-m range. Sites for stations CI.TUQ, CE.14560, and NM.BLO exceed the 300-m threshold, having respective values of 303, 380, and 660 m. As anticipated (see Section 2.1), the proximity of a recording location to a site often was controlled by manmade impediments or geophysical constraints. In the case of NM.BLO, the field crew acquired seismic data in much closer proximity to the seismic-station site, but data quality was such that additional data acquisition was required at an alternate location farther away from the seismic station. To this end, better quality seismic data were acquired along an array that was positioned more than 600 m away from NM.BLO.

The distribution of the V_{S30} values among the NEHRP Site Classes is shown in the histogram of figure 7. The mean, median, and range of measured V_{S30} values within each NEHRP Site Class, as well as for the entire dataset, are reported in table 4. Stations CI.DRE (Desert Research Extension Center) and CI.CLC (China Lake Naval Weapons Center) have, respectively, the lowest (196 m/s) and highest (1,464 m/s) V_{S30} values in this project. Most (104) of the measurements fall within NEHRP Site Class C (V_{S30} values between 360 and 760 m/s), similar to previous studies (Wills and Silva, 1998; Chiou and others, 2008; Yong and others, 2012). This likely reflects purposeful siting of earthquake monitoring stations in densely population regions where enclaves are typically located on sedimentary basins consisting of relatively softer materials. Site Class D (V_{S30} = 180–360 m/s) has 58 measurements, and Site Class B (V_{S30} = 760–1,500 m/s), with the fewest, has 29 measurements. No measurements were obtained that fall in Site Class E (V_{S30} < 180 m/s) or Class A (V_{S30} > 1,500 m/s).

It is, however, possible to reassign the NEHRP Site Classes for several stations by adjusting V_{S30} to account for the estimated emplacement depth of the SM sensor at each station (see Section 2.5.2.4). These adjusted values are listed in table 3 and provided in each site report. Inherently, an adjusted V_{S30} value will be larger than a measured V_{S30} value, as illustrated in figure 9 (denoted as $V_{S(Z,\,Z+30)}$). In proportion to a V_{S30} value, adjustments tend to increase with increasing values of V_{S30}, particularly for V_{S30} values larger than about 400 m/s. The largest adjustment (an increase of 93 percent) was for NM.BLO, which has a measured V_{S30} of 1,202 m/s, because the testing location had several meters of sediment overlying bedrock, whereas the seismic station is located directly on rock. On the basis of the adjusted V_{S30} values, the Site Classes of 14 stations would be reassigned: 4 stations would be reclassified from Site Class B to A, and 10 stations from Site Class C to B. A comparison of the distributions of V_{S30} and adjusted V_{S30} values is shown in figure 8.

For planning purposes, local geological conditions at each station were described using the binary system of "rock" or "soil" (see Section 2.0). Here (table 3), the "rock" category also includes many stations considered as "shallow-rock" sites, where the seismic station was previously expected to be directly located on rock. This classification scheme produces a near equal split of stations, where 52 percent are categorized as "rock" sites (table 3). This statistic, however, appears to be inconsistent with the observation that the distribution of V_{S30} values is skewed towards lower velocities (fig. 7), an observation that warrants further investigation. For the time being, two key factors also should be considered. First, the "rock" or "soil" categories are too broad to fully describe the complex geological conditions encountered in this project (rock sites include sediments and sedimentary rock of Tertiary age, or older crystalline rock, and do not consider extent of weathering). Nevertheless, as a logistical tool for planning purposes, it was the most convenient method for generalizing geological site conditions. Second, these classes typically were derived from geological maps or were assigned during onsite reconnaissance, where both sources are known to have critical limitations. For example, map-based assessments often cannot be well-constrained due to poor accuracy, low detail and (again) do not consider weathering. Field-based approaches for assessing local material properties can also be limited by extensive soil cover, such that depth to rock and rock type are not clear. An examination of the data in table 3 reveals a few stations (CI.GATR, CI.LJR, CI.SCZ2, NC.BBGB, NC.PMPB and PG.VPD) that initially were classified as "rock", but later were determined to have relatively lower than expected V_{S30} values corresponding to Site Class D. Four of these sites (CI.GATR, CI.SCZ2, NC.BBGB and PG.VPD) have Tertiary shale units at or near the surface, which could potentially weather to low velocity clay, hence the low V_{S30}. The other two sites were mapped as Mesozoic Franciscan Assemblage (NC.PMPB) and granitic rocks (CI.LJR) and are expected to have much higher V_{S30}. This result emphasizes the importance of acquiring measurement-based V_{S30} data whenever possible.

Cultural settings, the basis for establishing a classification system to categorize local noise conditions, were also used for planning purposes. Table 3 describes each station in terms of its assigned cultural class: rural (r), suburban (s), or urban (u). Regardless of the classification schemes used in this project, the MAS_RW technique was used at all stations.

The rural setting is most common, and includes 147 stations. In this low noise environment, active source surface- and body-wave techniques dominated the methods deployed. These methods, with the exception of the MAS_RW technique as the standalone approach at 12 soil sites, typically consisted of combinations of multiple techniques such as SASW, MAS_LW, MAS_RW, and seismic refraction (P- and S-wave). It is important to note that seismic-refraction models were only used to estimate V_{S30} when surface-wave techniques were not effective. The seismic-refraction technique was primarily used in a support role to identify depth to groundwater, depth to bedrock, quantify lateral velocity variation, or support V_{S30} estimates resulting from surface-wave data. As a result, V_{S30} values for 25 sites could not be estimated from MAS_RW data and instead were estimated from SASW, MAS_LW, and P- and/or S-wave seismic-refraction data. Passive surface-wave techniques (AM and/or ReMi^{TM}) were used at 10 rural stations and eight of these deployments contributed data for estimating V_{S30} values.

In moderate to low noise environments, 17 stations were categorized as situated in suburban settings. Although it is an intermediate category between the rural and urban classes, the suburban sites relied heavily on the same active surface-wave techniques applied at the rural sites. Interestingly, MAS_RW, MAS_LW, and P- and S-wave seismic-refraction techniques were used at seven suburban sites, primarily due to a thin sediment cover overlying rock. V_{S30} could only be estimated from MAS_RW at one of these sites. At the remaining sites, four sites were based on MAS_LW and two on S-wave refraction. Passive surface-wave techniques (AM and ReMi^{TM}) were used at only five suburban sites but always contributed data for estimating V_{S30} values (AM and ReMi^{TM} at three sites and AM only at two sites). At station CI.WNS, the MAS_RW and seismic P-wave refraction techniques were inadequate for modeling shallow V_S profile. Instead, the CI.WNS model was based on the PS-suspension logging technique (abbreviated as P in table 3) conducted by GEOVision©, Inc., for an earlier study.

At the 27 urban sites, passive surface-wave techniques (AM and ReMi^{TM}) were universally deployed, always in conjunction with MAS_RW, with the expectation that high levels of ambient noise generated by cultural sources would produce robust data for analysis. SASW data were also acquired at one urban site (CI.BAK) and P-wave seismic-refraction data at another urban site (CI.LAF). The seismic-refraction technique typically was not applied at urban sites because geologic conditions typically consist of soil rather than rock and the seismic-refraction technique was not expected to be effective in developed (asphalt or concrete surfaces), high ambient noise environments. V_{S30} values at all urban sites relied on V_S models from at least one of the two passive surface-wave techniques in combination with an active surface-wave technique.

The station V_{S30} values reported in table 3 (with the exception of CI.WNS, as previously noted) were calculated from V_S models derived from the various measurement techniques applied at each site. Techniques were either individually employed or multiple techniques were applied, in which case, and whenever appropriate, the same array configurations were shared (see Section 2.0). As previously mentioned, preference was always given to V_{S30} values estimated from surface-wave data—V_{S30} values estimated from seismic-refraction models were only utilized at 12 station sites where surface-wave methods were ineffective. Details on how particular methods were selected (or excluded) are provided in Section 2.3 and in individual station reports in appendix A. For example, the MAS_LW, MAS_RW, and seismic P- and S-wave refraction (collectively abbreviated as the MlMrSrpSrs method in table 3) techniques were used at station NC.MMX1, but only data from the P- and S-wave seismic-refraction models could be used to estimate the station V_{S30} value—coherent dispersion curves were not recoverable from the Rayleigh and Love data at this site. Station CE.24706 is another example where AM, MAS_RW, ReMi^{TM}, and P-wave seismic-refraction techniques (collectively abbreviated as the AMrRSrp method in table 3) were used; after careful consideration, data from the ReMi^{TM} technique were not included for developing a V_S model and estimating V_{S30} solution because the dispersion data derived from the array microtremor measurements were in better agreement with that derived from the MAS_RW measurements. As with all other sites, seismic-refraction models were not used to estimate V_{S30}, unless surface-wave methods were ineffective.

Figure 10 shows the number of, and in what proportion, various combinations of measurement techniques, including cases of when only one technique was used at the

sites. Although $MAS_R W$ (abbreviated as Mr in table 3) was used at all sites, it was the only technique applied at 12 soil sites and the only surface-wave technique applied at 73 rock sites. The SASW (abbreviated as S in table 3) technique, used in conjunction with the $MAS_R W$ technique at 29 sites, was applied almost exclusively on soil sites. Although not part of the scope of work, $MAS_L W$ (abbreviated as Ml in table 3) was used in an attempt to characterize 38 sites. Passive surface-wave techniques, including array microtremor (abbreviated as A in table 3), and the ReMi™ technique (abbreviated as R in table 3), were applied at 42 sites, primarily urban and suburban sites although occasionally at rural sites if there was a busy road near the site. The seismic-refraction technique (primarily P-wave and occasionally S-wave) was used at 122 sites, primarily in a support role to identify depth to groundwater or bedrock and quantify lateral velocity variation.

Figure 11 shows the number and proportion of various combinations of techniques (again including single techniques) that were selected from all surveys to derive the V_S models from which the V_{S30} values are calculated. There are five cases where all of the same techniques that were used in the field also were used to derive V_{S30}; in each case, the corresponding wedges in figures 10 and 11 have the same (non-gray) color. Note that while the $MAS_R W$ technique (abbreviated as Mr in table 3) was deployed as a standalone technique at 12 out of 191 stations (fig. 10), $MAS_R W$ models alone were used as the basis to estimate V_{S30} at 94 (nearly one-half) of all stations surveyed, primarily because seismic-refraction surveys were typically used in a supporting role and only used to estimate V_{S30} when various surface-wave techniques were ineffective. SASW data were combined with $MAS_R W$ data or used alone to characterize 21 sites. $MAS_L W$ models were used to characterize 17 sites and combined with $MAS_R W$ models to characterize an additional 5 sites. Active and passive surface-wave data were combined and used to estimate V_{S30} at 40 sites. A total of 12 sites could only be characterized using P- and/or S-wave seismic-refraction techniques.

4.0 Data and Resources

All data are available from the U.S. Geological Survey publication site for this report (*http://pubs.usgs.gov/of/2013/1102/*).

5.0 Acknowledgments

We are grateful to William Leith for support of the project through the 2009 American Recovery and Reinvestment Act (ARRA). Special thanks to: Jean Paul Ampuero, Dominic Assimaki, Rufus Catchings, Silvia Castellaro, Arthur Frankel, Susan Hough, Swaminathan Krishnan, and Walter Silva; who provided guidance in the development of the project. Beneficial remarks from John Boatwright and Nancy E. King, in addition to constructive comments by reviewers Christopher Stevens and Robert Graves greatly improved this report.

6.0 References Cited

Abrahamson, N., Atkinson, G., Boore, D., Bozorgnia, Y., Campbell, K., Chiou, B., Idriss, I.M., Silva, W., and Youngs, R., 2008, Comparisons of the NGA ground-motion relations: Earthquake Spectra, v. 24, no. 1, p. 45–66.

Aki, K., 1957, Space and time spectra of stationary stochastic waves, with special reference to microtremors: Bulletin of the Earthquake Research Institute, v. 35, p. 415–457.

Aki, K., 1965, A note on the use of microseism in determining the shallow structures of the Earth's crust: Geophysics, v. 30, p. 665–666.

Bettig, B., Bard, P.Y., Scherbaum, F., Riepl, J., Cotton, F., Cornou, C., and Hatzfeld, D., 2001, Analysis of dense array noise measurements using the modified spatial auto-correlation method (SPAC)—Application to the Grenoble area: Bollettino Di Geofisica Teorica Ed Appllicata**,** v. 42, p. 281–304.

Bodet, L., Abraham, O., and Clorennec, D., 2009, Near-offset effects on Rayleigh-wave dispersion measurements—Physical modeling: Journal of Applied Geophysics*,* v. 68, p. 95–103.

Boiero, D., and Socco, L.V., 2011, The meaning of surface wave dispersion curves in weakly laterally varying structures: Near Surface Geophysics, v. 9, no. 6, p. 561–570.

Boore, D.M., 2004, Can site response be predicted?: Journal of Earthquake Engineering, v. 8, no. 1, p. 1–41.

Boore, D.M., 2006, Determining subsurface shear-wave velocities—A review, *in* International Symposium on the Effects of Surface Geology on Seismic Motion, 3d, Grenoble, France, 2006, Proceedings: Grenoble, France, Paper Number 103, p. 1–21.

Boore, D.M., and Brown, L.T., 1998, Comparing shear-wave velocity profiles from inversion of surface-wave phase velocities with downhole measurements—Systematic differences between the CXW method and downhole measurements at six USC strong-motion sites: Seismological Research Letters, v. 69, no. 3, p. 222–229.

Boore, D.M., Joyner, W.B., and Fumal, T.E., 1993, Estimation of response spectra and peak accelerations from western North American earthquakes—An interim report, part 1: U.S. Geological Survey Open-File Report, p. 93–509, 69 p.

Boore, D.M., Joyner, W.B., and Fumal, T.E., 1994, Estimation of response spectra and peak accelerations from western North American earthquakes—An interim report, part 2: U.S. Geological Survey Open-File Report, p. 94–127, 40 p.

Boore, D.M., Joyner, W.B., and Fumal, T.E., 1997, Equations for estimating horizontal response spectra and peak acceleration from western North American earthquakes—A summary of recent work: Seismological Research Letters, v. 68, no. 1, p. 128–153.

Borcherdt, R.D., 1994, Estimates of site-dependent response spectra for design (methodology and justification): Earthquake Spectra, v. 10, no. 4, p. 617–653.

Borcherdt, R.D., 2002, Empirical evidence for acceleration-dependent amplification factors: Bulletin of the Seismological Society of America, v. 98, no. 4, p. 761–782.

Bragato, P.L., 2008, Limits for the improvement of ground-motion relations in Europe and the Middle East by accounting for site effects: Bulletin of the Seismological Society of America, v. 92, no. 2, p. 2,061–2,065.

Brown, L.T., Diehl, J.G., and Nigbor, R.L., 2000, A simplified method to measure average shear-wave velocity in the top 30 m (V_s30), *in* Proc. 6th International Conference on Seismic Zonation, Proceedings: Palm Springs, California, p. 1–6.

Building Seismic Safety Council, 2003, Recommended provisions for seismic regulations for new buildings and other structures, part 1—Provisions: Washington, D.C., Federal Emergency Management Agency, Report No. FEMA-450, 303 p.

Cakir, R., and Walsh, T.J., 2009, Shallow-seismic site characterizations of near-surface geology at 20 strongmotion stations in Washington state: U.S. Geological Survey/ National Earthquake Hazards Reduction Program, Technical Report No. G09AP00021, 40 p.

Cakir, R., and Walsh, T.J., 2012, Shallow-seismic site characterizations at 25 ANSS/PNSN stations and compilation of site-specific data for the entire strongmotion network in Washington and Oregon: U.S. Geological Survey/ National Earthquake Hazards Reduction Program, Technical Report No. G11AP20045, 61 p.

Capon, J., 1969, High-resolution frequency-wavenumber spectrum analysis: Proceedings of the Institute of Electrical and Electronics Engineers, v. 57, no. 8, p. 1,408–1,418.

Castellaro, S., and Mulargia, F., 2009, V_{S30} estimates using constrained H/V measurements: Bulletin of the Seismological Society of America, v. 99, no. 2A, p. 761–773.

Castellaro, S., Mulargia, F., and Rossi, P.L., 2008, Vs30: Proxy for seismic amplification?: Seismological Research Letters, v. 79, no. 4, p. 540–543.

Chiou, B., Darragh, R., Gregor, N., and Silva, W., 2008, NGA project strong-motion database: Earthquake Spectra, v. 24, no. 1, pp. 23–44.

Cho, I., Tada, T., and Shinozaki, Y., 2004, A new method to determine phase velocities of Rayleigh waves from microseisms: Geophysics, v. 69, no. 6, p. 1,535–1,561.

Comina, C., Foti, S., Boiero, D., and Socco, L.V., 2011, Reliability of $V_{S,30}$ evaluation from surface-wave tests: Journal of Geotechnical and Geoenvironmental Engineering, p. 579–586.

Cornou, C., Ohrnberger, M., Boore, D.M., Kudo, K., and Bard, P.-Y., 2006, Derivation of structural models from ambient vibration array recordings—Results from an international blind test, *in* International Symposium on the Effects of Surface Geology on Seismic Motion, 3d, Grenoble, France, 30 August–September 2006, Proceedings: Grenoble, France, Paper Number NBT, p. 1–93.

Cox, B.R., and Wood, C.M., 2011, Surface wave benchmarking exercise—Methodologies, results and uncertainties, *in* Georisk 2011—Geotechnical Risk Assessment and Management, Atlanta, Georgia, 2011, Proceedings: Silver Spring, Maryland, ASFE—The Geoprofessional Business Association, p. 845–852.

Delgado, J., Casado, C.L., Estévez, A., Giner, J., Cuenca, A., and Molina, S., 2000, Mapping soft soils in the Segura river valley (SE Spain)—A case study of microtremors as an exploration tool: Journal of Applied Geophysics, v. 45, p. 19–32.

Dobrin, M.S., and Savit, J., 1988, Introduction to Geophysical Prospecting: New York, McGraw-Hill Co., 876 p.

Dobry, R., Borcherdt, R.D., Crouse, C.B., Idriss, I.M., Joyner, W.B., Martin, G.R., Power, M.S., Rinne, E.E., and Seed, R.B., 2000, New site coefficients and site classification system used in recent building seismic code provisions: Earthquake Spectra, v. 16, no. 1, p. 41–67.

Ellefsen, K.J., 2003, Seg2_edit—A program for editing and manipulating SEG-2 files: U.S. Geological Survey Open-File Report 2003-141, 11 p.

Eslick, R., Tsoflias, G., and Steeples, D., 2007, Field investigations of Love waves in near-surface seismology: Geophysics, v. 73, no. 3, p. G1–G6.

Eurocode 8, 2004, Design of structures for earthquake resistance, part 1—General rules, seismic actions and rules for buildings, EN 1998: 1, European Committee for Standardization (CEN), accessed September 18, 2013 at *http://www.cen.eu/cenorm/homepage.htm*.

Foti, S.,Comina, C., and Boiero, D., 2007, Reliability of combined active and passive surface wave methods: Riv. Ital. Geotec., v. 41, no. 2, p. 39–47.

Gardner, L.W., 1967, Refraction seismograph profile interpretation, *in* Musgrave, A.W., ed., Seismic Refraction Prospecting: Tulsa, Oklahoma, Society of Exploration Geophysicists, p. 338–347.

Guzina, B.B., and Madyarov, A.I., 2003, A computational basis for the spectral analysis of Love waves, *in* Engineering Mechanics Conference, 16th, Seattle, Washington, 2003, Proceedings: American Society of Civil Engineers, University of Washington, Seattle, 9 p.

Hagedoorn, J.G., 1959, The plus-minus method of interpreting seismic refraction sections: Geophysical Prospecting, v. 7, p. 158–182.

Haines, S.S., 2007, A Hammer-impact, aluminum shear-wave seismic source: U.S. Geological Survey Open-File Report 2007-1406, 5 p.

Hales, F.W., 1958, An accurate graphical method for interpreting seismic refraction lines: Geophysical Prospecting, v. 6, p. 285–294.

Hasbrouck, W.P., 1983, Sketches of a hammer-impact, spiked-base, shear-wave source: U.S. Geological Survey Open-File Report 83-917, 7 p.

Haskell, N.A., 1953, The dispersion of surface waves on multilayered media: Bulletin of the Seismological Society of America, v. 43, p. 17–34.

Hawkins, L.V., 1961, The reciprocal method of routine shallow seismic refraction investigation: Geophysics, v. 26, p. 806–819.

Holtz, R.D., Kovacs, W.D., and Sheahan, T.C., 2010, An Introduction to Geotechnical Engineering (2nd ed.): Upper Saddle River, New Jersey, Prentice Hall, 864 p.

Ibs-von Seth, M., and Wohlenberg, J., 1999, Microtremor measurements used to map thickness of soft sediments: Bulletin of the Seismological Society of America, v. 89, no. 89, p. 250–259.

Joh, S.H., 1996, Advances in interpretation and analysis techniques for spectral-analysis-of-surface-waves (SASW) measurements: Austin, University of Texas, Ph.D. Dissertation, 240 p.

Joyner, W.B., Warrick, R.E., and Fumal, T.E., 1981, The effect of Quaternary alluvium on strong ground motion in the Coyote Lake, California, earthquake of 1979: Bulletin of the Seismological Society of America, v. 71, no. 4, p. 1,333–1,349.

Kausel, E., and Röesset, J.M., 1981, Stiffness matrices for layered soils: Bulletin of the Seismological Society of America, v. 71, no. 6, p. 1,743–1,761.

Kennett, B.L.N., 1974, Reflections, rays and reverberations: Bulletin of the Seismological Society of America, v. 64, no. 6, p. 1,685–1,696.

Konno, K., and Ohmachi, T., 1998, Ground-Motion Characteristics Estimated from Spectral Ratio between Horizontal and Vertical Components of Microtremor: Bulletin of the Seismological Society of America, v. 64, no. 1, p. 228–241.

Lai, C.G., and Rix, G.J., 1998, Simultaneous inversion of Rayleigh phase velocity and attenuation for near-surface site characterization: Georgia Institute of Technology, School of Civil and Environmental Engineering, 258 p.

Lai, C.G., and Rix, G.J., 1999, Inversion of multi-mode effective dispersion curves, *in* Jamiolkowski, M., Lancellotta, R., Lo Presti, D., eds., Prefailure deformation characteristics of geomaterials: Lisse, Netherlands, Balkema, p. 411–418.
Lacoss, R.T., Kelly, E.J., and Toksöz, M.N., 1969, Estimation of seismic noise structure using arrays: Geophysics, v. 34, p. 21–38.
Lane, J.D., Jr., 2009, Geotechnical site characterization using multi-channel analysis of Rayleigh and Love waves: Knoxville, University of Tennessee, Master of Science Thesis, 93 p.
Lankston, R.W., and Lankston, M.M., 1986, Obtaining multilayer reciprocal times through phantoming: Geophysics, v. 51, p. 45–49.
Lay, T., and Wallace, T.C., 1995, Model Global Seismology: Oxford, United Kingdom, Academic Press, 521 p.
Lee, V.W. and Trifunac, M.D., 2010, Should average shear-wave velocity in the top 30 m of soil be used to describe seismic amplification?: Soil Dynamics and Earthquake Engineering, v. 30, p. 1,250–1,258.
Lermo, J., and Chávez-García, F.J., 1994, Are microtremors useful in site response evaluation?: Bulletin of the Seismological Society of America, v. 84, no. 5, p. 1,350–1,364.
Li, J., and Rosenblad, B., 2011, Experimental study of near-field effects in multichannel array-based surface wave velocity measurements: Near Surface Geophysics, v. 9, p. 357–366.
Ling, S., and Okada, H., 1993, An extended use of the spatial correlation technique for the estimation of geological structure using microtremors, *in* Conference of the Society of Exploration Geophysicists Japan, 89th, Nagoya, Japan, 1993, Proceedings: Nagoya, Japan, Society of Exploration Geophysicists of Japan, p. 44–48 (in Japanese).
Louie, J.N., 2001, Faster, better—Shear-wave velocity to 100 meters depth from refraction microtremor arrays: Bulletin of the Seismological Society of America, v. 91, no. 2, p. 347–364.
Lu, L., and Zhang, B., 2006, Inversion of Rayleigh waves using a genetic algorithm in the presence of a low-velocity layer: Acoustical Physics, v. 52, no. 6, p. 701–712.
Ludwig, W.J., Nafe, J.E., and Drake, C.L., 1970, Seismic refraction, *in* Maxwell, A.E., ed., The Sea 4: New York, Wiley-Interscience, v. 4, p. 53–84.
Mari, J.L., 1984, Estimation of static corrections for shear-wave profiling using the dispersion properties of Love waves: Geophysics, v. 49, p. 1,169–1,179.
Martin, A.J., Shawver, J.B., and Diehl, J.G., 2006, Combined use of active and passive surface wave techniques for cost effective UBC/IBC site classification, Paper No. 1013, *in* U.S. National Conference on Earthquake Engineering, 8th, San Francisco, California, 2006, Proceedings: San Francisco, California, Earthquake Engineering Research Institute, Seismological Society of America, and the California Governor's Office of Emergency Services, 10 p.
McMechan, G.A., and Yedlin, M.J., 1981, Analysis of dispersive waves by wave field transformation: Geophysics, v. 46, p. 869–874.
Moss, R.E., 2008, Quantifying measurement uncertainty of thirty-meter shear-wave velocity: Bulletin of the Seismological Society of America, v. 98, no. 3, p. 1,399–1,411.

Mucciarelli, M., and Gallipoli, M.R., 2006, Comparison between VS30 and other estimates of site amplification in Italy: Geneva, Switzerland, 13th European Conference on Earthquake Engineering and Seismology and the 30th General Assembly of the ESC, accessed September 18, 2012 at *http://www.earth-prints.org/handle/2122/1945/*.

Nakamura, Y., 1989, A method for dynamic characteristics estimation of subsurface using microtremor on the ground surface: Quarterly Report of the Railway Technical Research Institute, v. 30, no. 1, p. 25–33.

Nazarian, S., and Desai, M.R., 1993, Automated surface wave method—Field testing: Journal of Geotechnical Engineering, v. 119, no. 7, p. 1,094–1,111.

Nogoshi, M., and Igarashi, T., 1971, On the amplitude characteristics of microtremor (part 2): Journal of the Seismological Society of Japan, v. 24, p. 26–40 (in Japanese).

Odum, J.K., Stephenson, W.J., and Williams, R.A., 2010, Predicted and observed spectral response from collocated shallow, active- and passive-source Vs data at Five ANSS sites, Illinois and Indiana, USA: Seismological Research Letters, v. 81, no. 6, p. 955–964.

Ohori, M., Nobata, A., and Wakamatsu, K., 2002, A comparison of ESAC and FK methods of estimating phase velocity using arbitrarily shaped microtremor arrays: Bulletin of the Seismological Society of America, v. 92, no. 6, p. 2,323–2,332.

Okada, H., 2003, The Microtremor Survey Method, Geophysical Monograph Series Number 12: Tulsa, Oklahoma, Society of Exploration Geophysicists, 135 p.

O'Neill, A., 2003, Full-waveform reflectivity for modeling, inversion and appraisal of seismic surface wave dispersion in shallow site investigations: Perth, University of Western Australia, Ph.D. Dissertation, 454 p.

Palmer, D., 1980, The generalized reciprocal method of seismic refraction interpretation: Tulsa, Oklahoma, Society of Exploration Geophysics, 104 p.

Park, C.B., Xia, J., and Miller, R.D., 1998, Imaging dispersion curves of surface waves on multi-channel record, Expanded Abstracts of 68th Annual International Meeting of the Society of Exploration Geophysics: The Society of Exploration Geophysics, p. 1,377–1,380.

Park, C.B., Miller, R.D., and Xia, J., 1999, Multichannel analysis of surface waves: Geophysics, v. 64, no. 3, p. 800–808.

Park, C.B., Miller, R.D., Ryden, N., Xia, J., and Ivanov, J., 2005, Combined use of active and passive surface waves: Journal of Environmental Engineering Geophysics, v. 10, no. 3, p. 323–334.

Pei, D., 2007, Modeling and inversion of dispersion curves of surface waves in shallow site investigations: Reno, University of Nevada, Ph.D Dissertation, 165 p.

Petersen, M.D., Frankel, A.D., Harmsen, S.C., Mueller, C.S., Haller, K.M., Wesson, R.L., Zeng, Y., Boyd, O.S., Perkins, D.M., Luco, N., Field, E.H., Wills, C.J., and Rukstales, K.S., 2008, Documentation for the 2008 update of the United States national seismic hazard maps: U.S. Geological Survey Open-File Report 2008-1128, 61 p.

Redpath, B.B., 1973, Seismic refraction exploration for engineering site investigations, U. S. Army Engineer Waterway Experiment Station (USAEWES) Explosive Excavation Research Laboratory (EERL): Livermore, California, Technical Report E-73-4, 51 p.

Rockwell, D.W., 1967, General wavefront method, *in* Musgrave, A.W., ed., Seismic Refraction Prospecting: Society of Exploration Geophysicists, pp. 363–415.
Röesset, J.M., Chang, D.W., and Stokoe, II, K.H., 1991, Comparison of 2-D and 3-D Models for Analysis of Surface Wave Tests, *in* International Conference on Soil Dynamics and Earthquake Engineering, 5th, Karlsruhe, Germany, Proceedings: Karlsruhe, Germany, American Society of Civil Engineers, 111–126 p.
Sánchez-Salinero, I., 1987, Analytical investigation of seismic methods used for engineering applications: Austin, University of Texas, Ph.D. Dissertation.
Safani, J., O'Neill, A., Matsuoka, T., and Sanada, Y., 2005, Applications of Love wave dispersion for improved shear-wave velocity imaging: Journal of Environmental Engineering Geophysics, v. 10, no. 2, p. 135–150.
Scheidegger, A., and Willmore, P.L., 1957, The use of a least square method for the interpretation of data from seismic surveys: Geophysics, v. 22, p. 9–22.
Schuler, J., 2008, Joint inversion of surface waves and refracted P- and S-waves: Zurich, ETH Swiss Federal Institute of Applied and Environmental Geophysics, Masters of Science thesis, 96 p.
Schuster, G.T., and Quintus-Bosz, A., 1993, Wavepath eikonal traveltime inversion—Theory: Geophysics, v. 58, no. 9, p. 1,314–1,323.
SESAME, 2004, Guidelines for the Implementation of the H/V spectral ratio technique on ambient vibrations—Measurements, processing and interpretation: European Commission, Project No. EVG1-CT-2000-00026, accessed September 2012, at *http://sesame-fp5.obs.ujf-grenoble.fr/*.
Socco, L.V., Strobbia, C., and Foti, S., 2002, Multimodal interpretation of surface wave data, *in* General Annual Meeting of Environmental and Engineering Geophysics-European Section (EEGS-ES), 8th, Proceedings: Aveiro, Portugal, Environmental and Engineering Geophysics- European Section, p. 21–25, accessed September 19, 2012 at *http://event.ua.pt/eegs_es/abstracts/ORAL/PAG021.PDF*.
Scott, J.B., Rasmussen, T., Luke, B., Taylor, W.J., Wagoner, J.L., Smith, S.B., and Louie, J.N., 2006, Shallow shear velocity and seismic microzonation of the urban Las Vegas, Nevada, basin: Bulleting of the Seismological Society of America, v. 96, no. 3, p. 1,068–1,077.
Sheriff, R.E., 2002, Encyclopedic dictionary of applied geophysics (4th ed.): Tulsa, Oklahoma, Society of Exploration Geophysics, Geophysical Reference Series 13, 429 p.
Stokoe II, K.H., Wright, S.G., Bay, J.A., and Roesset, J.M., 1994, Characterization of geotechnical sites by SASW method, *in* Woods, R.D., ed., Geophysical characterization of sites: International Science Publisher, New York, p. 15–26.
Stokoe, K.H., Cox, B.R., Lin, Y.-C., Jung, M.J., Menq, F.-Y., Bay, J.A., Rosenblad, R., and Wong, I., 2006, Use of intermediate to large vibrators as surface wave sources to evaluate V_s profiles for earthquake studies, *in* Annual Symposium on the Application of Geophysics to Engineering and Environment Problems, 19th, Seattle, Washington, 2006, Proceedings: Seattle, Washington, Society of Exploration Geophysicists, p. 57–74.

Stokoe, K.H., Nazarian, S., Rix, G.J., Sanchez-Salinero, I., Sheu, J.C., and Mok, Y.-J., 1988, In situ seismic testing of hard-to-sample soils by surface wave method, Proceedings (Earthquake Engineering and Soil Dynamics II—Recent Advances in Ground-motion Evaluation) of Geotechnical Engineering Division of the American Society of Civil Engineers (ASCE), Park City, Utah, 27–30 June 1988, Geotechnical Special Publication No. 20, pp. 264–278.

Strobbia, C., and Foti, S., 2006, Multi-offset phase analysis of surface wave data (MOPA): Journal of Applied Geophysics, v. 59, p. 300–313.

Telford, W.M., Geldart, L.P., and Sheriff, R.E., 1990, Applied Geophysics (2nd Ed.): New York, Cambridge University Press, 770 p.

Thompson, E.M., Baise, L.G., Kayen, R.E., Tanaka, Y., and Tanaka, H., 2010, A geostatistical approach to mapping site response spectral amplifications: Engineering Geology, v. 114, p. 330–342.

Thomson, W.T., 1950, Transmission of elastic waves through a stratified solid medium: Journal of Applied Physics, v. 21, no. 2, p. 89–93.

Tokimatsu, K., Tamura, S., and Kojima, H., 1992, Effects of multiple modes on Rayleigh wave dispersion characteristics: Journal of Geotechnical Engineering, v. 118, no. 10, p. 1,529–1,543.

Wills, C. J., and Silva, W., 1998, Shear-wave velocity characteristics of geologic units in California: Earthquake Spectra, v. 14, no. 3, p. 533–556.

Wyrobek, S.M., 1956, Application of delay and intercept times in the interpretation of multilayer time distance curves: Geophysical Prospecting, v. 4, p. 112–130.

Xia, J., Xu, Y., Luo, Y., Miller, R.D., Cakir, R., and Zeng, C., 2012, Advantages of using Multichannel analysis of Love waves (MALW) to estimate near-surface shear-wave velocity: Surveys in Geophysics, v. 33, no. 5, p. 841–860, accessed September 19, 2012 at *http://www.springerlink.com/content/du74825247366r88/fulltext.pdf*.

Xu, Y., Xia, J., and Miller, R.D., 2006, Quantitative estimation of minimum offset for multichannel surface wave survey with actively exciting source: Journal of Applied Geophysics, v. 59, p. 117–125.

Yong, A., Hough, S.E., Cox, B.R., Rathje, E.M., Bachhuber, J., Dulberg, R., Hulslander, D., Christiansen, L., and Abrams, M., 2011, Seismic-zonation of Port-au-Prince using pixel- and object-based imaging analysis methods on ASTER GDEM: Photogrammetry Engineering and Remote Sensing, v. 77, no. 9, p. 909–921.

Yong, A., Hough, S.E., Iwahashi, J., and Braverman, A., 2012, A terrain-based site-conditions map of California with implications for the contiguous United States: Bulletin of the Seismological Society of America, v. 102, no. 1, p. 114–128.

Yoon, S., and Rix, G.J., 2009, Near-field effects on Array-based surface wave methods with active sources: Journal of Geotech. Geoenviron. Eng., v. 135, no. 3, pp. 399–406.

Zhang, J., and Toksöz, M.N., 1998, Nonlinear refraction traveltime tomography: Geophysics, v. 63, p. 1,726–1,737.

Zywicki, D.J., 1999, Advanced signal Processing Methods Applied to Engineering Analysis of Seismic Surface Waves: Georgia Institute of Technology, Ph.D. Dissertation, 227 p.

Zywicki, D.J., and Rix, G.J., 2005, Mitigation of near-field effects for seismic surface wave velocity estimation with cylindrical beamformers: Journal of Geotechnical and Geoenvironmental Engineering, v. 131, no. 8, p. 970–977.

7.0 Glossary (Common Terms)

AM: Array Microtremor.
HVSR: Horizontal-to-Vertical-Spectral-Ratio.
MASW: Multi-channel-Analysis-of-Surface Waves (generic); however, generally assumed as Rayleigh-wave based.
MAS$_L$W: Multi-channel-Analysis-of-Surface Waves (Love-wave). Referred to as MALW in individual site reports.
MAS$_R$W: Multi-channel-Analysis-of-Surface-Waves (Rayleigh-wave). Referred to as MASW in individual site reports.
ReMi^{TM}: Refraction Microtremor.
SASW: Spectral-Analysis-of-Surface-Waves.
SAS$_L$W: Spectral-Analysis-of-Surface-Waves (Love-wave).
SM: strong motion.
V_L**:** Love-wave phase velocity
V_P: p-wave velocity.
V_R: Rayleigh-wave phase velocity.
V_{R40}: Rayleigh-wave phase velocity of the fundamental mode at 40-m wavelength.
V_S: shear-wave velocity.
V_{S30}: time-averaged shear-wave velocity in the upper 30 m from the surface.

8.0 Figures

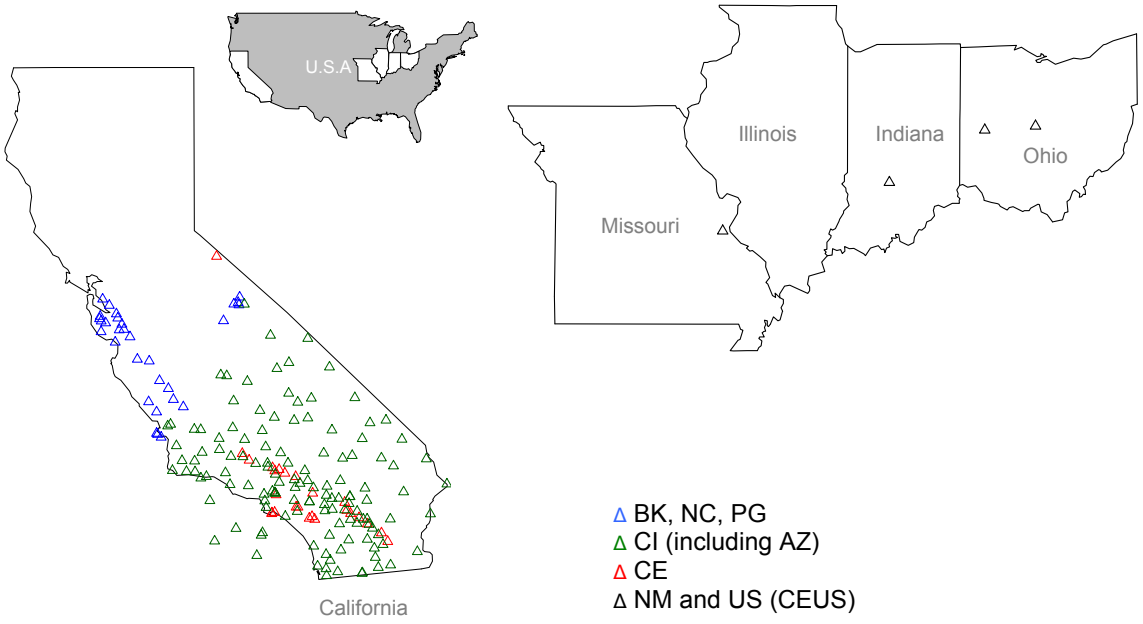

Figure 1. Maps of strong-motion stations in California and in the central-eastern U.S. Seismographic networks include: ANZA Seismic Network (AZ), U.C. Berkeley Digital Seismic Network (BK), California Geological Survey Seismic Network (CE), Southern California Seismic Network (CI), Northern California Seismic Network (NC), Pacific Gas and Electric Seismic Network (PG), and Central-Eastern United States (CEUS) Seismic Networks (NM and US).

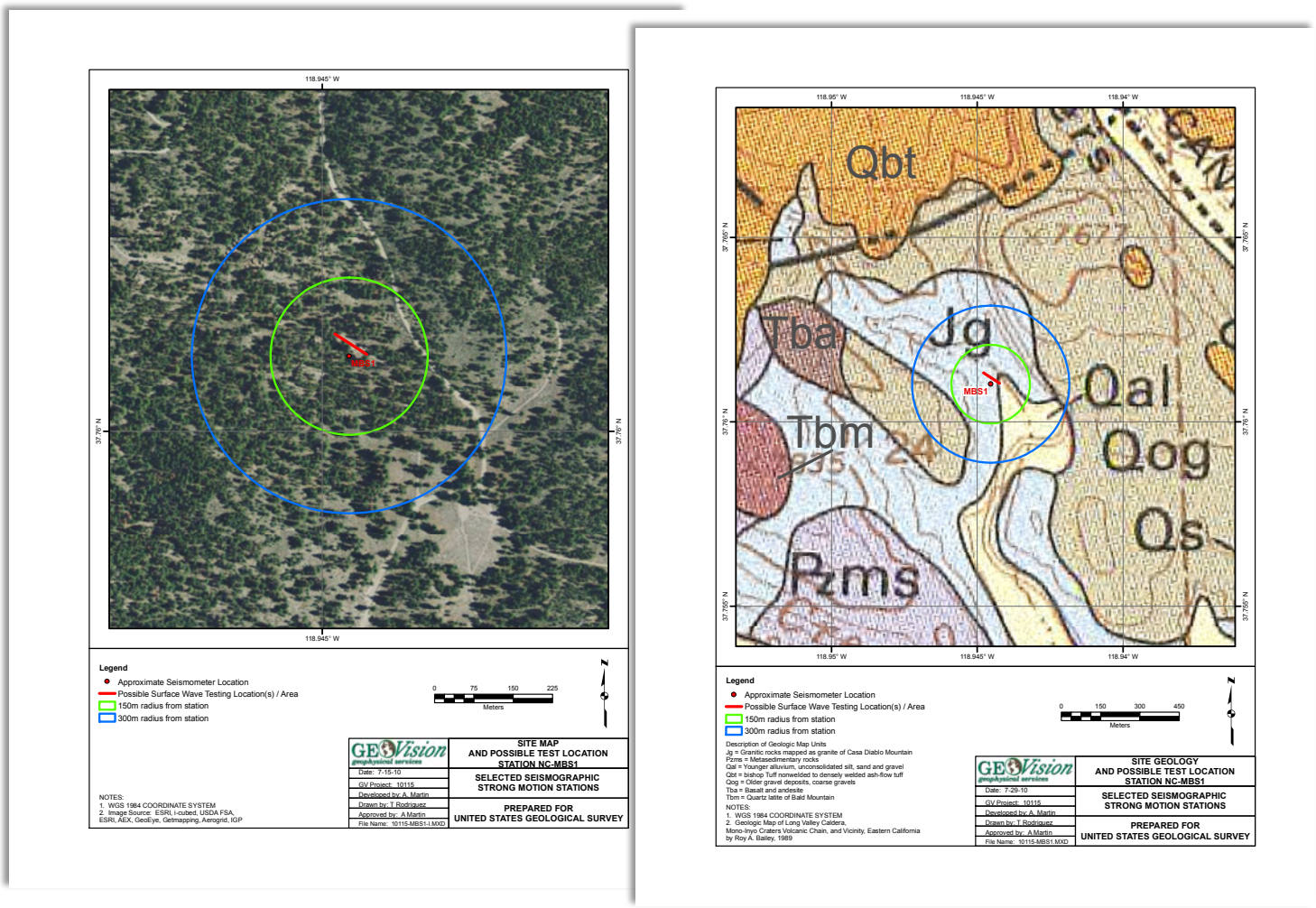

Figure 2. Samples of prerequisite maps: satellite-based (left) and geologic-based (right). The location (on record) of the station (red dot), proposed array site (red line), 150-meter radial threshold (green circle), and 300-meter threshold (blue circle) are shown on each map. Note that the maps are not at the same scale.

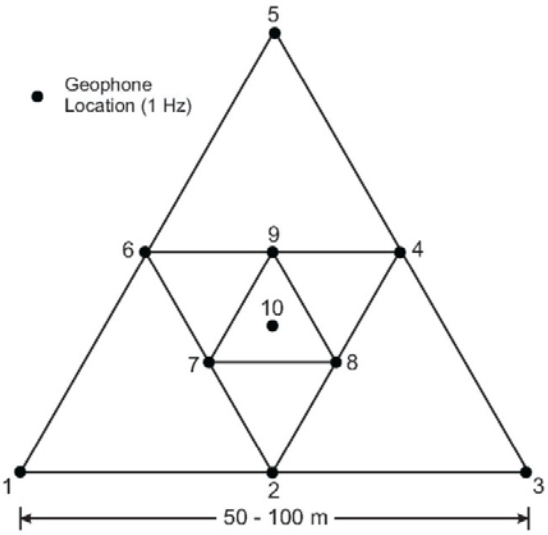

10 channel triangle array

Acquisition of passive surface wave data along 10 channel triangle array

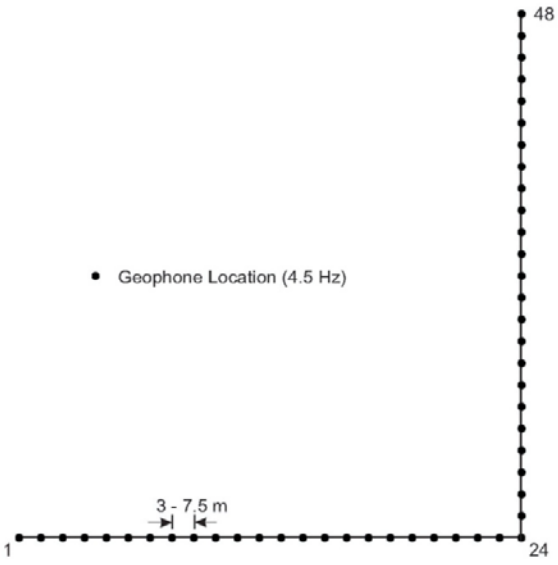

48 channel “L” shaped array

Acquisition of passive surface wave data along 48 channel “L” shaped array

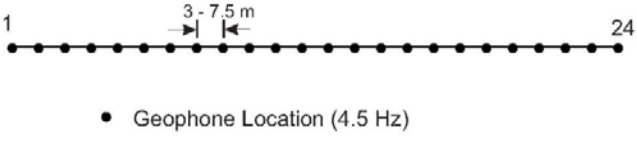

24 channel linear array

Acquisition of passive surface wave data along 24 channel linear array

Figure 3. Typical passive surface-wave arrays.

Nanometrics Trillium Compact seismometer (used for HVSR measurements at almost all sites).

Nanometrics Trillium Compact deployed in shallow hole.

Micromed Tromino ENGY (used for HVSR measurements at selected remote and/or shallow rock sites).

HVSR measurements (seismometer is covered to keep wind off sensor and sensor cable).

Figure 4. Horizontal-to-vertical spectral ratio (HVSR) instrumentation.

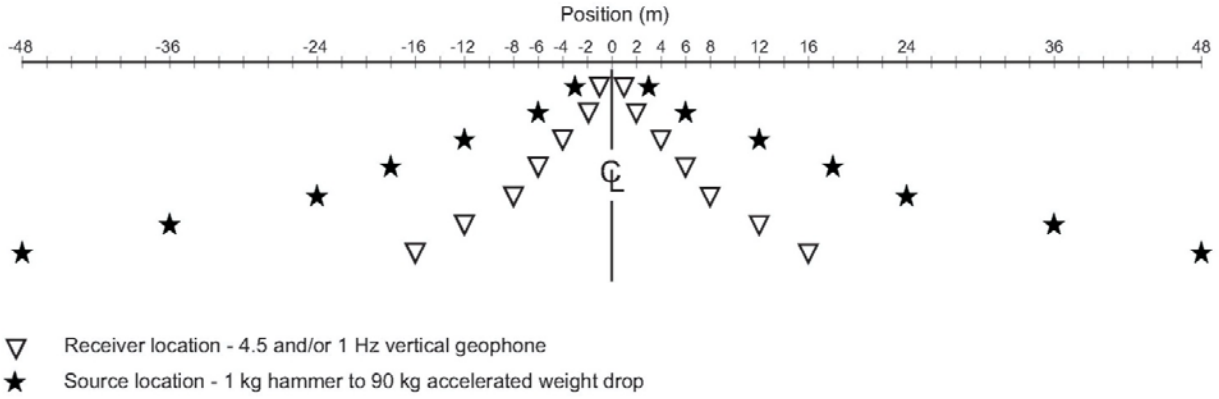

Typical Common Center Point SASW Array Geometry

HP Dynamic Signal Analyzer

Geospace 1 Hz vertical geophones

SASW array and 90 kg accelerated weight drop energy source (AWD)

Various hammer energy sources

Figure 5. SASW-array geometry and instrumentation.

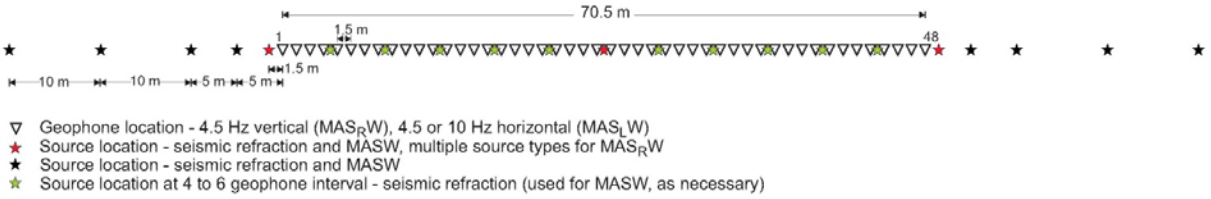

Typical MASW and seismic refraction array geometry.

Geometrics Geode seismograph.

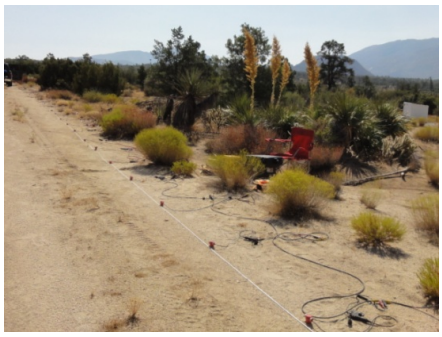

MAS_RW array with 4.5 Hz vertical geophones.

90 kg accelerated weight drop (AWD) energy source.

10 and 20 lb sledgehammer energy sources.

3 lb hammer energy source used for MAS_RW acquisition.

Horizontal traction plank and hammer for MAS_LW and S-wave refraction acquisition.

Hammer impact aluminum S-wave seismic source and 4.5 Hz horizontal geophones.

Figure 6. MASW and seismic-refraction survey design.

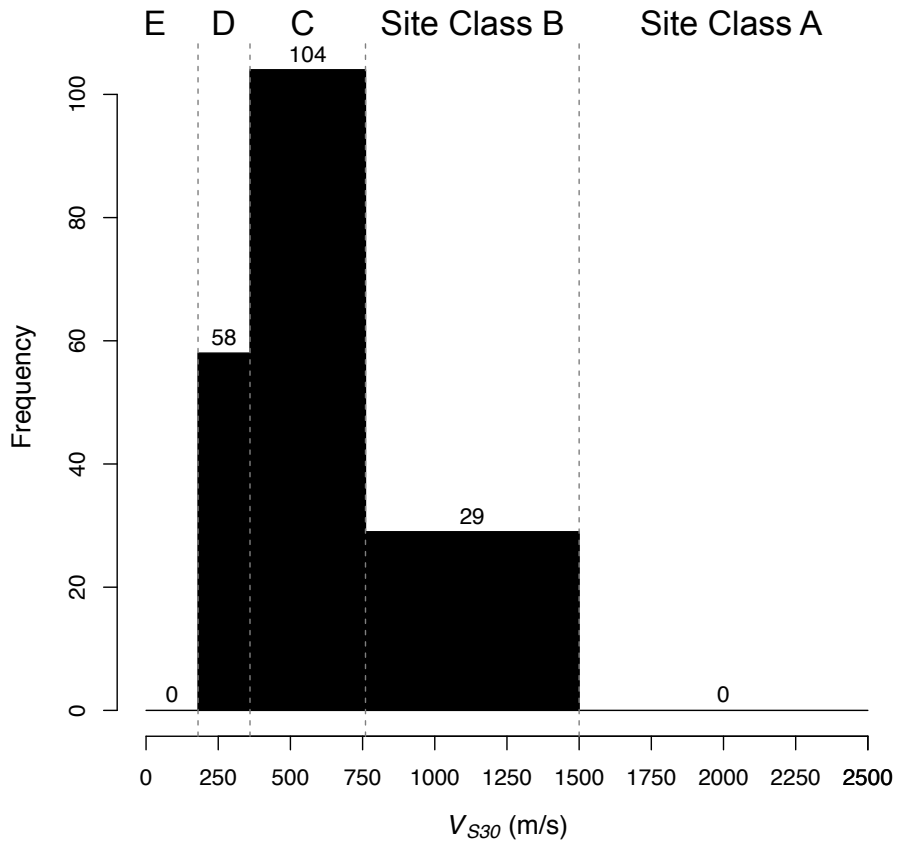

Figure 7. Histogram of 191 calculated V_{S30} values grouped into NEHRP site classes.

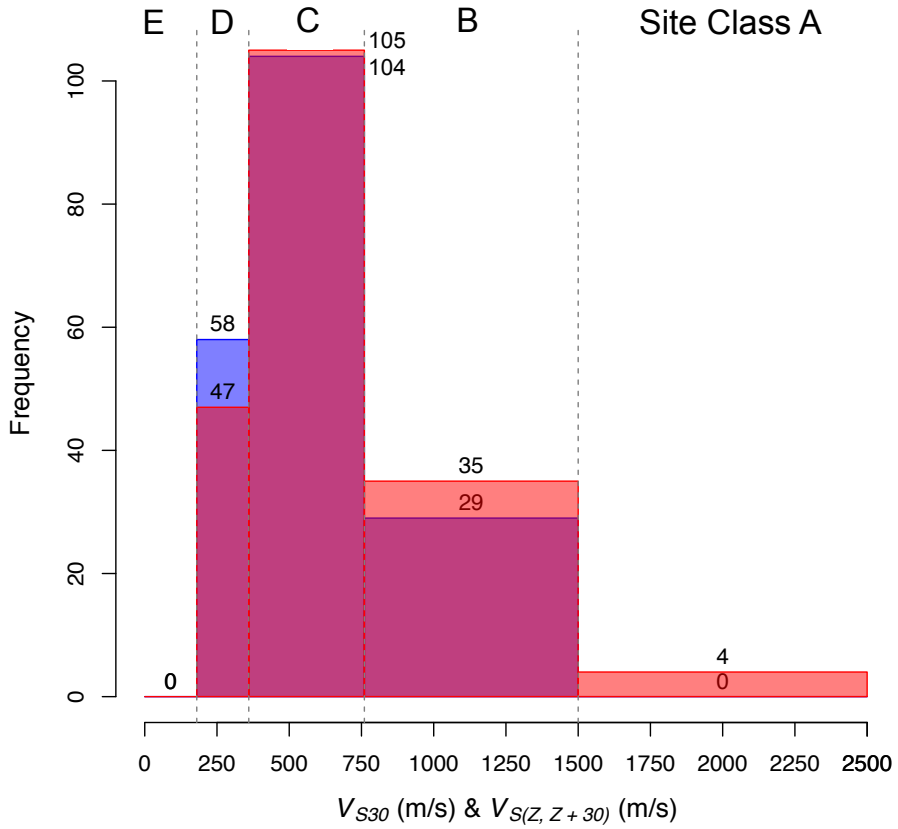

Figure 8. Histograms of V_{S30} values (blue) and adjusted $V_{S(Z, Z+30)}$ values (red) grouped into NEHRP site classes (overlapping areas shown as purple). Each type of data has 191 observations.

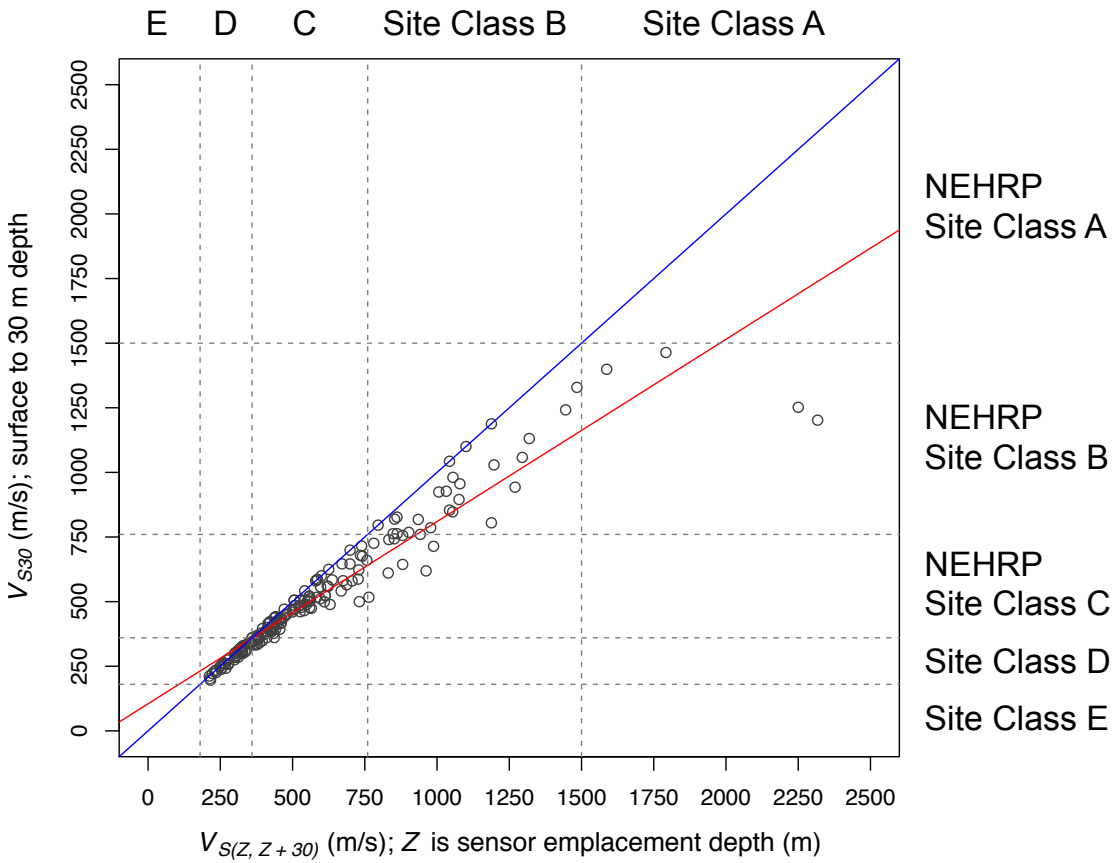

Figure 9. Plot of V_{S30} values versus adjusted $V_{S(Z, Z+30)}$ values, with velocity ranges of NEHRP site classes indicated. Blue line indicates the trend for a one-to-one relation and red line is the linear least-squares fit to the data.

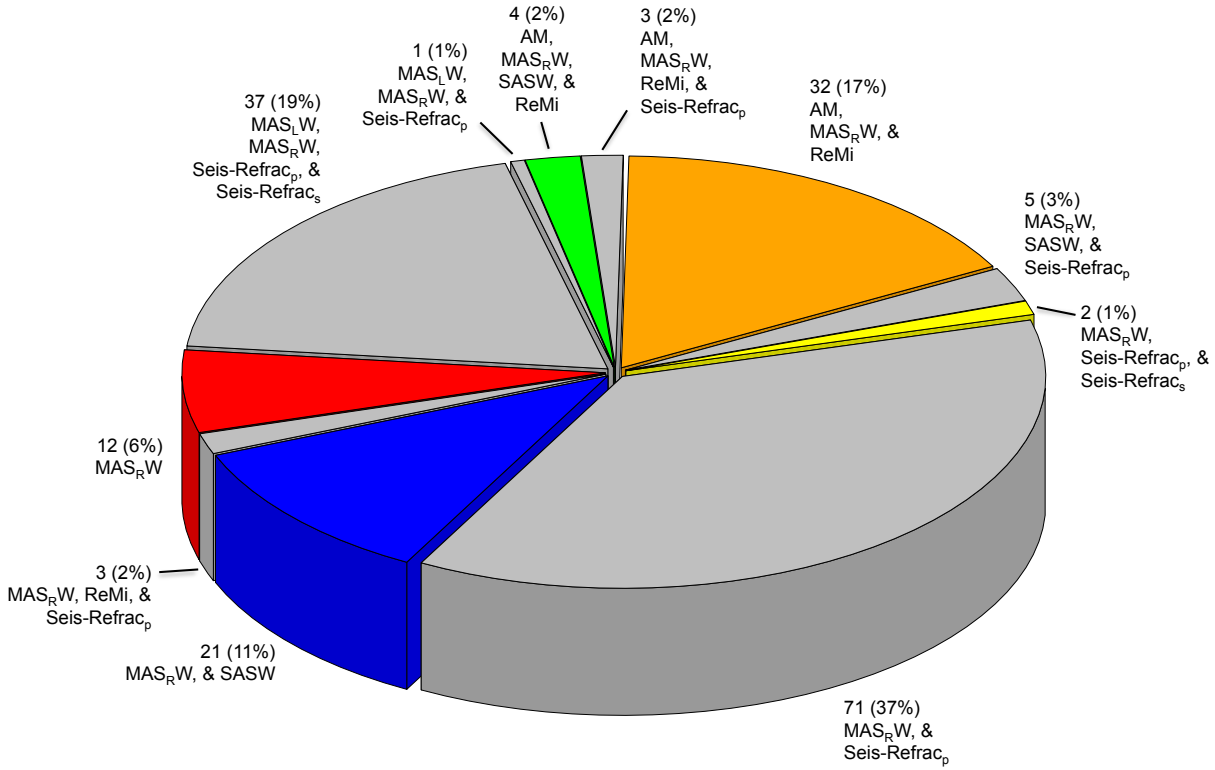

Figure 10. Distribution of the MASRW technique and various combined methods deployed at 191 strong-motion stations. The color scheme used in this and the next figure (fig. 11) is the same. Categories include the standalone technique of MASRW (red) or methods that combine: AM, MASRW, SASW and ReMi™ (green) aka AMrSR*; AM, MASRW and ReMi™ (orange) aka AMrR*; MASRW, Seis-RefracP (P-wave seismic refraction), and Seis-RefracS (Swave seismic refraction) (yellow) aka MrSrpSrs*; MASRW and SASW (blue) aka MrS*. The remaining categories (gray) in this figure differ in proportion to the gray color categories used to estimate V_{S30} values in figure 11.

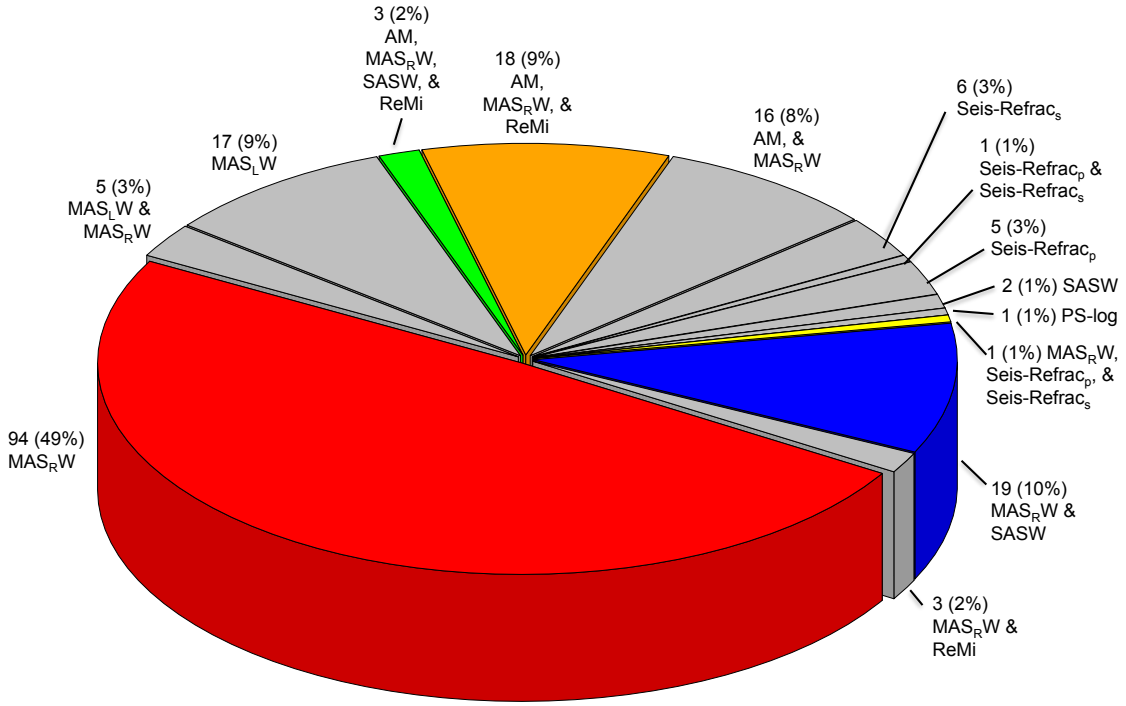

Figure 11. Distribution of the MASRW technique and various combined methods used to calculate V_{S30} values for 191 strong motion stations. The color scheme used to designate the various categories in this and the previous figure (fig. 10) is the same. Categories include the standalone technique of MASRW (red), or methods that combine: AM,MASRW, SASW, and ReMi™ (green) aka AMrSR*; AM, MASRW, and ReMi™ (orange) aka AMrR*; MASRW, Seis-RefracP (P-wave seismic refraction), and Seis-RefracS (S-wave seismic refraction) (yellow) aka MrSrpSrs*; MASRW, and SASW (blue) aka MrS*. The remaining categories (gray) in this figure are not proportionate to the gray color categories deployed in the field (fig. 10).

9.0 Tables

Table 1. Summary of seismographic networks and the number of strong-motion (SM) stations selected from each network.

Network	Number of Stations Proposed	Number of Stations Surveyed	Regional Seismographic Networks
CI	130	131	Southern California Seismographic Network (SCSN)
BK, NC, PG	30	30	Northern California Seismographic Network (NCSN)
CE	25	25	California Strong Motion Instrumentation Program (CSMIP), Statewide
NM, US	12	4	Center for Earthquake Research Institute (CERI), Central-eastern U.S. (CEUS)
AZ	0	1	ANZA, southern California

Table 2. Summary of site conditions and applicable geophysical techniques.

Types of Site Conditions	Geophysical Techniques							
	Passive Surface Wave Methods			Active Surface Wave Methods			Active Body Wave Methods	
	HVSR	AM	ReMi™	SASW	MAS_RW	MAS_LW	P-wave Seismic Refraction	S-wave Seismic Refraction
Rural Rock Sites	•			•	•	•	•	•
Suburban Rock Sites	•			•	•	•	•	•
Urban Rock Sites	•	•	•	•	•	•		
Rural Soil Sites	•			•	•	•	•	•
Suburban Soil Sites	•	•	•	•	•	•	•	•
Urban Soil Sites	•	•	•	•	•	•		

Table 3. Summary of results on site conditions at 191 strong-motion (SM) stations in California and the Central-Eastern United States (CEUS).

Network	Station	Latitude (°N) of Station	Longtitude (°E) of Station	Method(s)[1] Deployed at Site	Latitude (°N) of Site	Longtitude (°E) of Site	Distance[2] (m) from Station to Site	V_{S30} (m/s) by Method(s)	Adjusted V_{S30} (m/s)	Method(s)[3] for V_{S30}	NEHRP[4]	GMX[5]	Noise Condition[6]	Geologic Condition	Lithologic Condition[7]
AZ	PFO	33.61167	-116.45943	MlMrSrpSrs	33.61158	-116.45631	289	763	848	MlMr	B/C	IGA	r	rock	qd
BK	KCC	37.32363	-119.3187	MrSrp	37.32554	-119.32096	292	1252	2250	Mr	B/A	FGA	r	rock	Kmg
BK	RAMR	35.63604	-120.86978	MrSrp	35.63638	-120.86894	85	300	328	Mr	D	IMD	r	rock	Tml
CE	11023	33.2389	-115.513	AMrR	33.23892	-115.51188	104	212	212	AMrR	D	AHD	r	soil	Ql
CE	11625	33.56409	-115.98763	MrS	33.56452	-115.98786	52	318	318	MrS	D	IHD	r	soil	Qa
CE	11684	33.39799	-115.65859	MrS	33.3978	-115.65711	139	202	202	MrS	D	IHD	r	soil	Ql
CE	12076	33.6781	-116.178	AMrR	33.67716	-116.18063	265	263	263	AMrR	D	AHD	u	soil	Qa-Qc
CE	12108	33.8149	-116.4612	AMrR	33.81686	-116.46087	220	301	301	AMrR	D	AHD	u	soil	Qs
CE	12149	33.9617	-116.5105	AMrR	33.96058	-116.50927	168	359	385	AMr	D/C	AHD	u	soil	Qa
CE	12952	33.7577	-116.374	AMrR	33.75711	-116.37476	96	274	274	AMr	D	AHD	u	soil	Qs
CE	13096	33.69884	-117.2664	MrSrp	33.69986	-117.26691	123	646	699	Mr	C	ATA	r	rock	Mzp/Mzq
CE	13099	33.8759	-117.5928	AMrR	33.87752	-117.59272	180	420	420	AMrR	C	AHD	u	soil	Qyfg
CE	13100	33.87559	-117.63549	AMrR	33.8753	-117.63428	116	341	357	AMrR	D/C	AQD	s	soil	Qoa
CE	13922	33.6691	-117.33225	MlMrSrpSrs	33.66783	-117.33272	148	581	675	Ml	C	AHB/AQB	s	soil	Qyva
CE	13929	33.64911	-117.20525	MlMrSrpSrs	33.64952	-117.20593	78	565	565	Ml	C	AQB	s	soil	Qof
CE	14241	33.77725	-118.13308	AMrR	33.77612	-118.13458	187	282	282	AMr	D	IQD	u	soil	Qops
CE	14395	33.75513	-118.20115	AMrR	33.75569	-118.20177	85	230	230	AMr	D	IHD	u	soil	Qal
CE	14560	33.76856	-118.19654	AMrR	33.77036	-118.20004	380	322	322	AMrR	D	IQD/IHD	u	soil	Qt
CE	23063	34.5025	-117.897	AMrRSrp	34.50277	-117.89898	184	506	506	AMr	C	AQD	r	soil	Qo
CE	23897	34.13322	-117.25281	MlMrSrpSrs	34.13281	-117.25429	144	584	584	Mr	C	AHB/AKB	s	soil	Qa/ps
CE	23958	34.43942	-117.64644	AMrR	34.43891	-117.64823	174	423	443	AMr	C	AHD	r	soil	Qa
CE	24029	34.10353	-118.10011	AMrR	34.10445	-118.10065	114	369	377	AMr	C/D	AQD	u	soil	Qae
CE	24644	34.74335	-118.72493	MrSrp	34.74374	-118.72481	45	421	421	Mr	C	IGB	r	rock	grd
CE	24706	34.546507	-118.129614	AMrRSrp	34.54856	-118.12929	230	468	501	AMr	C	IHB/GHB	s	soil	Qa
CE	24775	34.86637	-118.88359	Mr	34.86419	-118.88294	250	437	437	Mr	C	IHC/GHB/GHC	r	soil	Qa
CE	24965	34.5702	-118.02999	AMrR	34.5717	-118.02852	214	326	326	AMrR	D	AHD	u	soil	Qa
CE	24967	34.60335	-118.18212	AMrR	34.60481	-118.18229	163	330	330	AMrR	D	AHD	u	soil	Qa
CE	65097	38.51455	-119.47973	AMrSR	38.5133	-119.48065	160	415	415	AMrSR	C	AHD/AQD	r	soil	Qf3-2
CI	ADO	34.55048	-117.43399	MrS	34.55152	-117.434	116	375	400	Mr	C	IHD	r	soil	Qa
CI	ALP	34.68702	-118.29947	Mr	34.68673	-118.30004	61	347	362	Mr	D/C	IHD	r	soil	Qa
CI	ARV	35.1269	-118.83009	MrSrp	35.12636	-118.8305	71	348	395	Mr	D/C	IMD	r	rock	Tsm/Tbe
CI	BAK	35.34444	-119.10445	AMrSR	35.34326	-119.10489	137	275	299	AMrSR	D	IHD	u	soil	Qf
CI	BAR	32.68005	-116.67215	MrSrp	32.67949	-116.67264	77	511	559	Mr	C	AGB/AGA	r	rock	gr
CI	BBR	34.26215	-116.92084	Mr	34.26223	-116.92141	53	356	380	Mr	D/C	IHD	r	soil	Qyf3
CI	BBS	33.92139	-116.98058	AMrR	33.92053	-116.98124	113	341	352	AMrR	D	IQD	u	soil	Qoa
CI	BC3	33.65513	-115.45364	MrSrp	33.65578	-115.45368	72	763	862	Mr	B	IGA	r	rock	gr
CI	BCW	34.9401	-119.41314	MrSrp	34.93946	-119.41227	107	305	335	Mr	D	IOC	r	rock	Tsi
CI	BEL	34.00057	-115.99816	MrSrp	33.99932	-115.99776	144	796	796	Mr	B	INA	r	rock	gn
CI	BFS	34.23883	-117.65853	MlMrSrpSrs	34.23827	-117.65841	63	500	731	Mr	C	IHB/IHA	r	soil	Qg
CI	BHP	33.99053	-118.36171	AMrR	33.98983	-118.3615	80	300	323	AMr	D	IQD	u	soil	Qoa
CI	BLA	34.06948	-116.38896	MrSrp	34.0693	-116.39028	123	524	613	Mr	C	IQB	r	soil	Qoa
CI	BLA2	34.06931	-116.38993	MrSrp	34.0693	-116.39028	32	524	613	Mr	C	IQB	r	soil	Qoa
CI	BLY	33.7503	-114.52373	MrSrp	33.7515	-114.52389	134	1029	1197	Mr	B	IZA	r	rock	PlPs
CI	BOM	33.36465	-115.72963	MrS	33.36488	-115.7291	55	202	214	MrS	D	IHD/IQD	r	soil	Ql/Tl
CI	BOR	33.2682	-116.41716	MrSrp	33.26748	-116.41608	128	619	962	Mr	C/B	IHA/IHB	r	soil	Qf
CI	BTP	34.68218	-118.57406	MrSrp	34.68258	-118.57461	67	461	526	Mr	C	INB	r	rock	gn
CI	CAC	34.13678	-118.12199	AMrR	34.13608	-118.12136	97	399	433	AMr	C	CQD	u	soil	Qof
CI	CAR	35.30819	-119.84583	MrSSrp	35.3083	-119.84672	82	310	339	Mr	D	IHD	r	soil	Qa
CI	CBC	34.13972	-118.12715	AMrR	34.13885	-118.12787	117	361	437	AMrR	C/D	GQD	u	soil	Qof
CI	CCC	35.52475	-117.36459	Mr	35.52513	-117.36339	117	432	461	Mr	C	IQD	r	soil	sa

Table 3. Summary of results on site conditions at 191 strong-motion (SM) stations in California and the Central-Eastern United States (CEUS) —continued.

Network	Station	Latitude (°N) of Station	Longtitude (°E) of Station	Method(s)[1] Deployed at Site	Latitude (°N) of Site	Longtitude (°E) of Site	Distance[2] (m) from Station to Site	V_{S30} (m/s) by Method(s)	Adjusted V_{S30} (m/s)	Method(s)[3] for V_{S30}	NEHRP[4]	GMX[5]	Noise Condition[6]	Geologic Condition	Lithologic Condition[7]
CI	CGO	36.54998	-117.80294	MrSrp	36.54883	-117.80201	152	715	739	Mr	C	IZA	r	rock	Mr
CI	CHF	34.33338	-118.02588	MrSrp	34.33273	-118.02647	90	927	1032	Mr	B	IGA	r	rock	lgd
CI	CHN	33.9988	-117.68026	AMrR	33.99775	-117.68087	130	292	307	AMrR	D	IHD	u	soil	Qyf3a
CI	CIA	33.40184	-118.41496	MrSrp	33.40283	-118.41602	148	505	526	Mr	C	INB	r	rock	m/ub
CI	CLC	35.81574	-117.59751	MlMrSrpSrs	35.81487	-117.59603	165	1464	1792	Srp	A/B	IGA	r	rock	gr
CI	CRP	34.13624	-118.12705	AMrR	34.13603	-118.12887	169	340	474	AMrR	D/C	FQD	u	soil	Qof
CI	CTC	33.65511	-115.99004	Mr	33.65474	-115.9892	88	370	396	Mr	C	IQD	r	soil	Qo-u
CI	CTD	33.35486	-118.44436	MrSrp	33.3559	-118.44457	117	756	881	Mr	C/B	IFA	r	rock	KJf
CI	CWC	36.43907	-118.08048	MrSrp	36.43903	-118.08106	52	580	580	Mr	C	AHB	r	soil	Qal
CI	DAN	34.63725	-115.3801	MrS	34.63784	-115.38094	101	477	528	MrS	C	IHD	r	soil	Qya
CI	DNR	33.56667	-116.63056	MrRSrp	33.56715	-116.63082	59	361	411	MrR	C	IJC/IZC	r	rock	Qa/ms
CI	DPP	32.99886	-116.94188	MlMrSrpSrs	32.99878	-116.94074	107	611	830	Ml	C/B	IGA/IGB	r	rock	Kg-gr
CI	DRE	32.80535	-115.44677	MrS	32.80502	-115.4463	57	196	216	Mr	D	IHD	r	soil	Ql
CI	DSC	35.14255	-116.10395	MlMrSrpSrs	35.14202	-116.10419	63	1329	1484	Srs	B	AHA/AZA	r	rock	Qal/C
CI	DVT	32.65877	-116.09984	MrRSrp	32.65902	-116.10019	43	625	625	MrR	C	AGA/AGB	r	rock	qd
CI	EDW2	34.8811	-117.99388	MlMrSrpSrs	34.88215	-117.99309	137	1242	1445	Ml	B	IGA	r	rock	qm
CI	EML	32.89083	-116.84566	MlMrSrpSrs	32.89049	-116.84699	130	805	1188	Srs	B	IVA	r	rock	Kmv
CI	ERR	33.11645	-115.82271	MrS	33.11615	-115.82256	36	238	253	MrS	D	IHD	r	soil	Qc
CI	FHO	34.09355	-116.93588	MrSrp	34.09277	-116.93719	149	416	460	Mr	C	IQB/IQC	r	soil	Qot
CI	FIG	34.72832	-119.98803	MlMrSrpSrs	34.72804	-119.98779	38	489	630	Ml	C	IFB/IFA	r	rock	fg
CI	FUR	36.46717	-116.86322	MrSSrp	36.46713	-116.8643	97	433	456	Mr	C	IQD/IPD	r	soil	Tft/Qai
CI	GATR	34.55266	-120.50235	MrSrp	34.55314	-120.50194	65	338	345	Mr	D/C	IMB/IMD	r	rock	Tml
CI	GLA	33.05149	-114.82706	MrSrp	33.05048	-114.82716	113	743	834	Mr	C/B	IVA	r	rock	Tvb
CI	GMR	34.78457	-115.65994	MlMrSrpSrs	34.78493	-115.65962	50	943	1270	Srs	B	IHA/IGA	r	rock	Qaag-Qyag/Qha/fpg/Qhs
CI	GOR	33.1537	-117.22921	MrSrp	33.15448	-117.22935	88	559	623	Mr	C	IGA/IGB	s	rock	Kt
CI	GRA	36.99606	-117.36615	MrSSrp	36.99644	-117.36605	43	386	407	S	C	IHD	r	soil	Qal
CI	GSC	35.30177	-116.80574	MrSrp	35.30142	-116.80642	73	679	735	Mr	C	AGA	r	rock	gr
CI	HEC	34.82954	-116.33637	MrSrp	34.82984	-116.33694	62	726	781	Mr	C/B	IGA	r	rock	gqm
CI	IDO	33.79673	-116.22153	MrSrp	33.79789	-116.22243	153	557	597	Mr	C	IQD	r	soil	Qo
CI	IKP	32.65012	-116.10948	MrSrp	32.65055	-116.1094	48	1058	1295	Mr	B	IGA	r	rock	qd
CI	IRM	34.15734	-115.14513	MrSrp	34.15773	-115.14488	49	981	1055	Mr	B	IGA	r	rock	Kii
CI	ISA	35.66278	-118.47403	MrSrp	35.66223	-118.47436	68	644	823	Mr	C/B	FGA	r	rock	Kma
CI	JEM	33.08098	-116.59755	MrSrp	33.07979	-116.59831	150	501	559	Mr	C	IGB/INB	r	rock	Js
CI	JRC2	35.98249	-117.80885	MrSSrp	35.98221	-117.80835	55	623	729	S	C	IVB	r	rock	Qtu
CI	JVA	34.36622	-116.61266	MrS	34.36608	-116.61227	39	383	417	Mr	C	IHD	r	soil	Qa
CI	LAF	33.86889	-118.33143	AMrRSrp	33.86838	-118.3323	98	257	278	AMrR	D	IHD	u	soil	Qae
CI	LCP	34.73547	-120.27984	MrSSrp	34.73601	-120.27922	83	259	267	MrS	D	IHD	r	soil	Qa/QTp
CI	LDF	35.13066	-115.18416	Mr	35.13094	-115.18452	45	453	487	Mr	C	IHD	r	soil	Qal
CI	LDR	34.9906	-118.34156	Mr	34.99089	-118.34027	122	378	415	Mr	C	IQD	r	soil	Qoa
CI	LEV	34.61404	-118.28929	MlMrSrpSrs	34.61343	-118.28877	83	505	505	Ml	C	AHB	s	soil	Qa
CI	LJR	34.80762	-118.86775	MlMrSrpSrs	34.8079	-118.86784	32	303	325	Ml	D	IGB/IGC	r	rock	qm
CI	LPC	34.31478	-117.54642	MrSrp	34.3149	-117.54511	121	506	542	Mr	C	IHB/IHC	r	soil	Qa
CI	LRL	35.47954	-117.68212	MrSrp	35.4792	-117.68304	91	511	596	Mr	C	IGA/IGB	r	rock	qd
CI	LUG	34.3656	-117.36683	MrS	34.3651	-117.36696	57	365	381	MrS	C/D	IQD	r	soil	Qof
CI	MCT	34.22645	-116.04073	MlMrSrpSrs	34.22641	-116.03938	124	1188	1188	Srp	B	IGA	r	rock	bqm
CI	MIK	34.13688	-118.12601	AMrR	34.13505	-118.12419	264	333	376	AMrR	D/C	DQD/EQD/GQD	u	soil	Qof
CI	MLAC	37.63019	-118.83605	AMrSR	37.6304	-118.83596	25	308	322	MrS	D	IQD	r	soil	Qoa
CI	MPI	34.8126	-119.14523	MrSrp	34.81301	-119.14641	117	452	536	Mr	C	IGB	r	rock	gr
CI	MPP	34.88848	-119.81362	MrSrp	34.88795	-119.81378	61	522	558	Mr	C	IEB/ILB	r	rock	Tss
CI	MSC	34.03852	-116.64795	MlMrSrpSrs	34.03978	-116.64845	147	377	434	Ml	C	INB	r	rock	gn

Table 3. Summary of results on site conditions at 191 strong-motion (SM) stations in California and the Central-Eastern United States (CEUS) —continued.

Network	Station	Latitude (°N) of Station	Longtitude (°E) of Station	Method(s)[1] Deployed at Site	Latitude (°N) of Site	Longtitude (°E) of Site	Distance[2] (m) from Station to Site	V_{S30} (m/s) by Method(s)	Adjusted V_{S30} (m/s)	Method(s)[3] for V_{S30}	NEHRP[4]	GMX[5]	Noise Condition[6]	Geologic Condition	Lithologic Condition[7]
CI	MSJ	33.80801	-116.96789	AMrR	33.80941	-116.96769	157	244	255	AMrR	D	IHD	s	soil	Qa
CI	MTP	35.48434	-115.5532	MrSrp	35.48552	-115.5534	132	956	1079	Mr	B	IZA	r	rock	epC
CI	NBS	34.78035	-116.55798	MrS	34.78127	-116.55733	118	419	461	MrS	C	IHD	r	soil	Qa
CI	NEE2	34.76754	-114.61883	MrS	34.76713	-114.6194	69	401	427	MrS	C	IQD/IHD	r	soil	Qayi
CI	NJQ	34.53412	-120.17737	MrS	34.53489	-120.17646	119	297	314	MrS	D	IHD	r	soil	Qa
CI	NSS2	33.55553	-115.94586	MrS	33.55453	-115.94624	117	352	377	MrS	D/C	IHD	r	soil	Qa
CI	OLP	32.60778	-116.93036	MrSrp	32.60781	-116.93083	44	489	548	Mr	C	IVB	r	rock	KJmv
CI	PASC	34.17141	-118.18523	MrSrp	34.17198	-118.18704	178	714	988	Mr	C/B	IGA	s	rock	qd
CI	PDM	34.3033	-114.14218	MrSrp	34.30269	-114.14411	190	1312	1560	Mr	B/A	INA	r	rock	pCc
CI	PHL	35.40773	-120.54556	MlMrSrpSrs	35.40828	-120.5459	68	384	428	Mr	C	IHB	r	soil	Qg
CI	PLC	33.82436	-116.51195	AMrR	33.82408	-116.51238	50	346	371	AMr	D/C	IHD	u	soil	Qa
CI	PLM	33.35361	-116.86265	MrSrp	33.35398	-116.86302	54	465	540	Mr	C	AGB	r	rock	gr
CI	PLS	33.7953	-117.60906	MrSrp	33.79505	-117.6088	37	699	699	Mr	C	AJA	r	rock	Jbc
CI	PMD	33.64785	-116.37769	MrSrp	33.64695	-116.37871	138	786	978	Mr	B	IGA	r	rock	qd
CI	RCT	36.30523	-119.24384	AMrSR	36.30629	-119.2439	118	282	301	AMrSR	D	IHD	r	soil	Qf
CI	RRX	34.87499	-116.99683	MrS	34.87498	-116.99575	99	372	396	MrS	C	IQD/IHD	r	soil	Qa/Qof
CI	RSB	33.97327	-117.32755	AMrR	33.97343	-117.32638	109	360	663	AMr	C/D	FHC	u	soil	Qya
CI	RSS	33.97327	-117.32755	AMrR	33.97425	-117.32795	115	360	360	AMr	C/D	LHC/BHC	u	soil	Qya
CI	RXH	33.18313	-115.62257	MrSrp	33.18379	-115.62283	77	309	324	Mr	D	IVD	r	rock	Qrv-r
CI	SAL	33.2801	-115.98585	Mr	33.28034	-115.98654	69	253	264	Mr	D	IQD	r	soil	Qoa
CI	SAN	33.70442	-117.88669	AMrR	33.70636	-117.88731	223	222	222	AMr	D	BHD/GHD	u	soil	Qal
CI	SBB2	34.68844	-117.8242	MrSrp	34.68803	-117.82466	62	1131	1319	Mr	B	IGA	r	rock	qm
CI	SBC	34.44076	-119.71492	AMrR	34.44143	-119.71379	128	485	507	MrR	C	CHD	u	soil	Qa
CI	SBI	33.48046	-119.02986	MrSrp	33.48005	-119.02961	51	854	1043	Mr	B	KQA/KVA	r	soil	Qoa/Tv
CI	SBPX	34.23246	-117.2349	MrSrp	34.23242	-117.23545	51	393	441	Mr	C	IGB	r	rock	gr
CI	SCI2	32.9799	-118.54697	MlMrSrpSrs	32.98019	-118.54774	79	442	442	Mr	C	AQB/AVB	r	soil	Qso/Tr
CI	SCZ2	33.99549	-119.63514	Mr	33.99512	-119.63417	98	313	325	Mr	D	IMD	r	rock	Tm
CI	SDG	32.784	-117.13805	MrSrp	32.78417	-117.13655	141	439	439	Mr	C	IQD	s	soil	Qoa
CI	SDR	32.73561	-116.94241	MlMrSrpSrs	32.73557	-116.94374	124	827	861	Srs	B/C	KGA/IGA	s	rock	Kgt
CI	SHO	35.89964	-116.27518	MrS	35.89972	-116.27479	36	356	377	MrS	D/C	IQD	r	soil	Qalo
CI	SIO	34.29224	-119.16694	AMrR	34.29197	-119.16707	32	249	249	AMr	D	AHD	s	soil	Qhf
CI	SLA	35.89095	-117.28332	MrSrp	35.89184	-117.28312	101	482	521	Mr	C	IVA	r	rock	Tv
CI	SLB	33.48519	-115.86643	MrS	33.48492	-115.86669	39	336	377	MrS	D/C	IHD	r	soil	Qcb/Qa-Qc
CI	SLR	33.83359	-116.79737	MlMrSrpSrs	33.83317	-116.79764	53	503	617	MlMr	C	IGB	r	rock	qdi
CI	SMM	35.31402	-119.99579	MrS	35.3146	-119.99565	66	225	235	MrS	D	IHD	r	soil	Qa
CI	SMR	35.37688	-120.61236	MrSrp	35.37665	-120.61286	52	847	1054	Mr	B	IKA	r	rock	Kas/Ka
CI	SMV	34.27091	-118.74407	AMrR	34.2692	-118.74286	220	260	278	AMr	D	AHD	u	soil	Qa
CI	SMW	35.01108	-120.40997	MrSrp	35.01016	-120.40962	107	676	742	Mr	C	IVA	r	rock	Tov
CI	SNCC	33.24786	-119.52437	MrSrp	33.2476	-119.52353	83	541	668	Mr	C	FQB	r	soil	Qs/Qt
CI	SNO	34.03515	-116.80778	MrSrp	34.03563	-116.80879	107	503	553	Mr	C	INB	r	rock	gn
CI	SPG2	36.20057	-118.76624	MrSrp	36.20012	-118.76663	61	910	987	Mr	B	IGA	r	rock	gr
CI	SWS	32.94503	-115.7999	MrSrp	32.94516	-115.80059	66	525	587	Mr	C	IGA/IGB	r	rock	gd
CI	SYP	34.52775	-119.97834	MrSrp	34.52646	-119.9791	159	440	470	Mr	C	IEB	r	rock	Tma
CI	TA2	34.38206	-117.67819	MrSrp	34.38287	-117.67908	122	565	565	Mr	C	ANB	r	rock	ml/gn
CI	TEH	35.2913	-118.42079	MrSrpSrs	35.29032	-118.42094	110	895	1076	MrSrpSrs	B	IGA	r	rock	gr
CI	TFT	35.1458	-119.41941	MrS	35.14518	-119.41871	94	332	367	MrS	D	AHD/KHD	r	soil	Qa
CI	THM	33.65066	-116.07734	Mr	33.65043	-116.07634	96	452	480	Mr	C	IQD	r	soil	Qo-u
CI	TIN	37.05422	-118.23009	MrRSrp	37.05652	-118.23132	278	396	396	Mr	C	AVD/APD	r	rock	Tb/Ts
CI	TOR	33.57526	-116.22584	MrSrpSrs	33.57571	-116.22679	101	1100	1100	Srp	B	IGA	r	rock	qdi
CI	TUQ	35.43584	-115.92389	MrSrp	35.43644	-115.92715	303	819	853	Mr	B	IGA	r	rock	gr

Table 3. Summary of results on site conditions at 191 strong-motion (SM) stations in California and the Central-Eastern United States (CEUS) —continued.

Network	Station	Latitude (°N) of Station	Longtitude (°E) of Station	Method(s)[1] Deployed at Site	Latitude (°N) of Site	Longtitude (°E) of Site	Distance[2] (m) from Station to Site	V_{S30} (m/s) by Method(s)	Adjusted V_{S30} (m/s)	Method(s)[3] for V_{S30}	NEHRP[4]	GMX[5]	Noise Condition[6]	Geologic Condition	Lithologic Condition[7]
CI	USB	34.41357	-119.84368	AMrR	34.41463	-119.84549	204	300	300	AMrR	D	IQD/FQD	u	soil	Qoa
CI	VCS	34.48372	-118.11781	AMrR	34.48447	-118.11749	88	405	433	AMrR	C	IQC	r	soil	Qoa
CI	VES	35.84088	-119.08489	MrS	35.84067	-119.08428	60	393	456	Mr	C	IQD	r	soil	Qoa3/QTkr
CI	VOG	36.32097	-119.38224	AMrR	36.32044	-119.38314	100	341	358	AMrR	D/C	IHD	s	soil	Qf
CI	WBS	35.53664	-118.14035	MrSrp	35.53716	-118.14091	77	402	426	Mr	C	IGA	r	rock	gr
CI	WES	32.75905	-115.73152	MrS	32.75945	-115.73273	122	242	269	MrS	D	IHD	r	soil	Qa-Qc
CI	WGR	34.51085	-119.27407	MlMrSrpSrs	34.51104	-119.27369	41	660	757	Srs	C/B	IKA	r	rock	Qg/Kush
CI	WNS	34.11395	-118.37967	MrSrp	34.11352	-118.37966	48	1043	1043	P	B	BGA	s	rock	qd
CI	WWC	33.94068	-116.40876	MrSrp	33.94134	-116.40834	83	587	727	Mr	C	INB	r	rock	sg
NC	BBGB	36.57849	-121.03956	MlMrSrpSrs	36.57752	-121.03955	108	285	312	Ml	D	IED	r	rock	Tk
NC	BJOB	36.61087	-121.31467	MrSrp	36.61041	-121.31403	77	486	528	Mr	C	IGB	r	rock	Kqd
NC	CADB	37.16346	-121.62645	MlMrSrp	37.16371	-121.62737	86	600	600	Ml	C	IFA	r	rock	fg
NC	CAL	37.45035	-121.80037	MrSrp	37.45063	-121.79928	101	519	557	Mr	C	IHB/IFB	r	rock	Qls/fs
NC	CCOB	37.25898	-121.67311	MlMrSrpSrs	37.25796	-121.67343	117	400	414	Mr	C	IKD	r	rock	Kp
NC	CHR	37.37289	-121.76887	MrSrp	37.37268	-121.76826	59	471	471	Mr	C	IMB	r	rock	Tbr
NC	CNI	37.60791	-121.96442	MlMrSrpSrs	37.60754	-121.96465	46	517	584	MlMr	C	IKB	r	rock	Ko
NC	CSL	37.7241	-122.11927	MrSrp	37.72349	-122.11865	87	378	391	Mr	C	IVB/IVC	r	rock	Jsv
NC	HCAB	37.02533	-121.48476	MrSrp	37.02599	-121.48514	81	646	671	Mr	C	IEB/ILB	r	rock	Tsh
NC	JBMB	37.31861	-122.15314	MlMrSrpSrs	37.31792	-122.15347	82	584	637	Ml	C	IFB	r	rock	fs/fg
NC	JBNB	37.12043	-122.1552	MlMrSrpSrs	37.12014	-122.1564	111	760	942	Ml	B	IGA	r	rock	qd
NC	JELB	36.92742	-121.82765	Mr	36.92684	-121.82651	120	323	323	Mr	D	IQD	r	soil	Qar
NC	JFP	37.36045	-122.18986	MlMrSrpSrs	37.36001	-122.19081	97	437	456	Ml	C	IFB	r	rock	fg
NC	JLAB	37.15432	-121.73467	MlMrSrpSrs	37.15422	-121.73517	46	477	559	Mr	C	IFB	r	rock	fm
NC	JSFB	37.40372	-122.17596	MrSrp	37.40333	-122.17617	47	432	463	Mr	C	IMB	r	rock	Tm
NC	JSGB	37.28395	-122.05026	Mr	37.28362	-122.05012	39	376	400	Mr	C	IQD	r	soil	Qoa/Qsc
NC	MBS1	37.76099	-118.94467	MlMrSrpSrs	37.7604	-118.94436	71	740	833	Srp	C/B	IGA	r	rock	Jg
NC	MDPB	37.63227	-119.07935	MrSrp	37.63188	-119.0792	45	580	706	Mr	C	IVA	r	rock	Qad
NC	MMLB	37.65909	-118.97907	MrSrp	37.65924	-118.97949	41	317	317	Mr	D	IVD	r	rock	Qmrm
NC	MMX1	37.61711	-118.95976	MlMrSrpSrs	37.61685	-118.96114	125	565	687	SrpSrs	C	IZA	r	rock	Pzms
NC	PAGB	35.73065	-120.24986	MlMrSrpSrs	35.73016	-120.24907	90	473	510	Ml	C	IJB	r	rock	sp
NC	PHOB	35.86661	-120.4796	MrS	35.86724	-120.48005	81	376	404	MrS	C	IQD/IPD	r	soil	QTp
NC	PHSB	35.82402	-121.05396	MrSrp	35.82379	-121.05484	83	422	422	Mr	C	IMB	r	rock	Tvq
NC	PMPB	36.2159	-120.80126	MlMrSrpSrs	36.21634	-120.80196	80	308	308	Ml	D	IFD	r	rock	fm
NC	PSM	36.0688	-120.59618	MrSrp	36.06897	-120.59556	59	560	620	Srp	C	IMB/IMA	r	rock	Tm
NM	BLO	39.1719	-86.5222	MlMrSrpSrs	39.17766	-86.52406	660	1202	2317	Srs	B/A	DZA	s	rock	M2
NM	JCMO	38.25749	-90.55847	MlMrSrpSrs	38.25676	-90.55864	83	768	902	Ml	B	LZA	s	rock	Ojc
NM	PIOH	40.15802	-84.21151	MrSrp	40.15879	-84.21123	89	416	447	Mr	C	IZB	s	rock	Oc
PG	DCD	35.22132	-120.84669	MlMrSrpSrs	35.22184	-120.84633	66	517	764	Ml	C/B	IVA	r	rock	Tov
PG	SHD	35.16898	-120.76319	MlMrSrpSrs	35.16931	-120.76366	56	818	935	MlMr	B	IKA	r	rock	Kas
PG	VPD	35.23979	-120.86951	MrSrp	35.23998	-120.87017	64	262	262	Mr	D	IMD	r	rock	Tm
US	ACSO	40.23228	-82.98202	MlMrSrpSrs	40.23205	-82.9813	66	417	467	MlMr	C	IZB	r	rock	Doh

[1,3]Abbreviations for methods with the following techniques:
A for array microtremor (AM);
Mr for multi-channel analysis of surface (Raleigh) waves (MAS_RW);
Ml for multi-channel analysis of surface (Love) waves (MAS_LW);
P for PS-suspension logging;
R for refraction microtremor (ReMi™);
S for spectral analysis of surface waves (SASW);
Srp for seismic refraction, P-wave; and
Srs for seismic refraction, S-wave.

[2]Distance is measured from station coordinates (on record) to coordinate of farthest end-point of array.

[4]NEHRP Site Class exceptions: Whenever an estimated V_{S30} value falls close to a Site Class boundary, the assigned Site Class is denoted by "/" such that the first letter is the actual Site Class according to the calculated V_{S30} value and second letter is the recommended Site Class based on the proximity of the V_{S30} value to the adjacent Site Class boundary.

[5]GMX for Geomatrix code; the same basis (see NEHRP Site Class exceptions) for the usage of "/" is also applied here.

[6]Noise conditions are based on the cultural settings of rural (r), suburban (s) and urban (u).

[7]See the individual site reports for lithologic units.

Table 4. Summary of National Earthquake Hazards Reduction Program site classes and measured V_{S30} values for strong motion stations in California and the central-eastern U.S.

NEHRP Site Class	NEHRP V_{S30} (m/s) Ranges	Number of Stations	Max. V_{S30} (m/s)	Min. V_{S30} (m/s)	Mean V_{S30} (m/s)	Median V_{S30} (m/s)	Std. Deviation of V_{S30} (m/s)
A	> 1500	0	NA	NA	NA	NA	NA
B	760 - 1500	29	1464	763	994	943	199
C	360 - 760	104	760	361	502	485	105
D	180 - 360	58	360	196	296	304	46
E	< 180	0	NA	NA	NA	NA	NA

10.0 Appendix A

The complete collection of site reports is appended alphabetically based on the station's network code followed by the station code. These reports can be found as of2013-1102_appendix_a.pdf at *http://pubs.usgs.gov/of/2013/1102/*.